Selective photocytotoxicity of anthrols on cancer stem-like cells: the effect of quinone methides or reactive oxygen species

Lidija Uzelac,[1]† Đani Škalamera,[2]† Kata Mlinarić-Majerski,[2] Nikola Basarić,[2]* and Marijeta Kralj[1]*

[1] Division of Molecular Medicine, Ruđer Bošković Institute, Bijenička cesta 54, 10 000 Zagreb, Croatia. Fax: + 385 1 4561 010; Tel: +385 1 4571 235

[2] Department of Organic Chemistry and Biochemistry, Ruđer Bošković Institute, Bijenička cesta 54, 10 000 Zagreb, Croatia. Fax: + 385 1 4680 195; Tel: +385 1 4561 141

† The first two authors contributed equally to the preparation of this manuscript.

*Authors of correspondence: Dr. Marijeta Kralj, e-mail: marijeta.kralj@irb.hr; Dr. Nikola Basarić, e-mail: nbasaric@irb.hr

Graphical abstract

photochemically generated
Quinone methide

alkylation of nucleophiles in cytosol

- H₂O

Sensitisation of singlet oxygen formation

³O₂

ROS
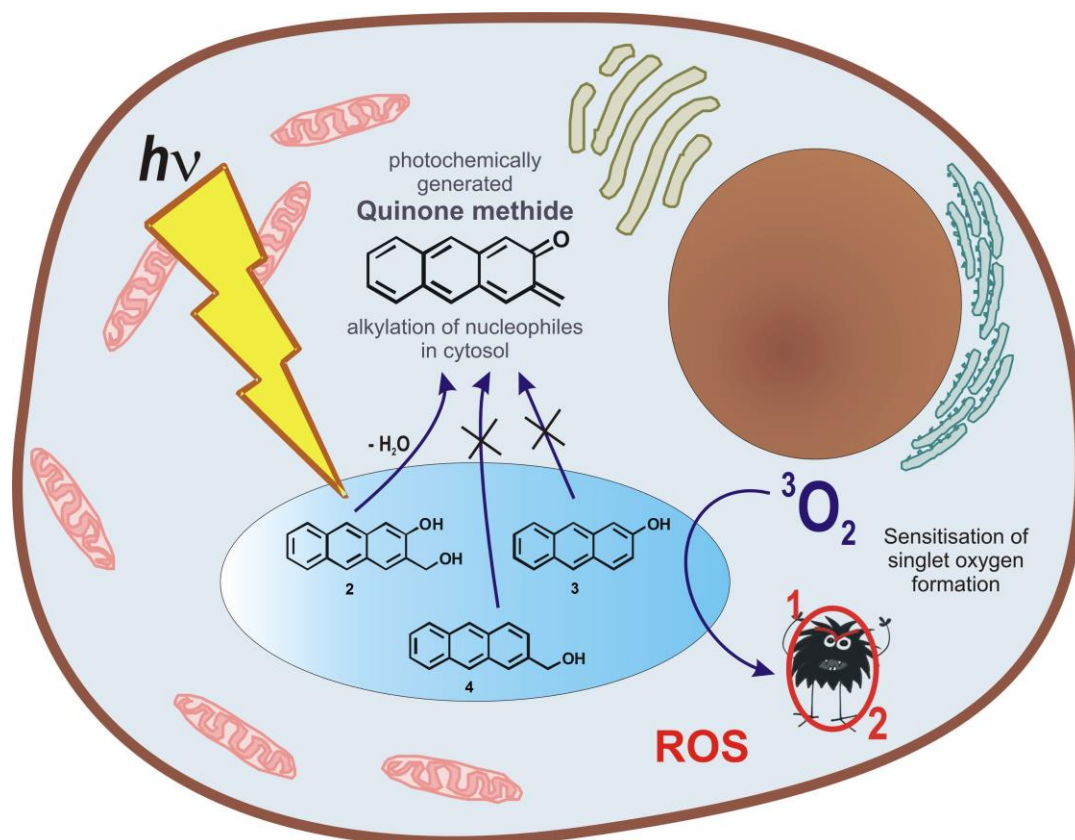
Abstract

Cancer stem cells (CSCs) are a subpopulation of cancer cells that share properties of embryonic stem cells like pluripotency and self-renewal and show increased resistance to chemo- and radiotherapy. Targeting CSC, rather than cancer cells in general, is a novel and promising strategy for cancer treatment. Novel therapeutic approaches, such as photodynamic therapy (PDT) have been investigated. A promising group of phototherapeutic agents are reactive intermediates - quinone methides (QMs). This study describes preparation of QM precursor, 2-hydroxy-3-hydroxymethylanthracene (**2**) and a detailed photochemical and photobiological investigation on similar anthracene derivatives **3** and **4**. Upon photoexcitation with near visible light at $\lambda > 400$ nm **1** and **2** give QMs, that were detected by laser flash photolysis and their reactivity with nucleophiles has been demonstrated in the preparative irradiation experiments where the corresponding adducts were isolated and characterized. **3** and **4** cannot undergo photodehydration and deliver QM, but lead to the formation of phenoxyl radical and singlet oxygen, respectively. The activity of **1**-**4** was tested on a panel of human tumor cell lines, while special attention was devoted to demonstrate their potential selectivity towards the cells with CSC-like properties (HMLEshEcad). Upon the irradiation of cell lines treated with **1**-**4**, an enhancement of antiproliferative activity was demonstrated, but the DNA was not the target molecule. Confocal microscopy revealed that these compounds entered the cell and, upon irradiation, reacted with cellular membranes. Our experiments demonstrated moderate selectivity of **2** and **4** towards CSC-like cells, while necrosis was shown to be a dominant cell death mechanism. Especially interesting was the selectivity of **4** that produced higher levels of ROS in CSC-like cells, which forms the basis for further research on cancer phototherapy, as well as for

the elucidation of the underlying mechanism of the observed CSC selectivity based on oxidative stress activation.

Key words: antiproliferative activity, cancer stem cells, photodehydration, quinone methides, reactive oxygen species, singlet oxygen

Introduction

Cancer stem cells (CSCs) are a subpopulation of cancer cells that share properties of embryonic stem cells like pluripotency and self-renewal. Importantly, CSCs show increased resistance to chemo- and radiotherapy. The molecular pathways contributing to drug resistance are not clear, but are related to enhanced survival pathways, elevated expression of drug transporters (e.g. P-gp) or depletion of oxygen radicals. CSCs surviving primary treatment frequently cause relapse; thus, attacking the CSC should abolish the tumor's ability to recur or metastasize. Targeting CSCs, rather than cancer cells in general, is a novel and highly promising strategy for cancer treatment [1,2].

CSCs are difficult to propagate outside of the tumor environment, because CSCs generally comprise only small minorities within cancer cell populations. Therefore, standard high-throughput cell viability assays applied to bulk cancer cells populations cannot identify agents with CSC-specific toxicity. Accordingly, screening for agents that preferentially kill CSCs depends on the ability to propagate stable, highly enriched populations of CSCs in vitro, or on using specific model cell lines enriched with cells that have stem-like properties [3]. Recently, a model of CSCs that experimentally induces the epithelial-mesenchymal transition (EMT) in breast epithelial cells was established and a large library of compounds was screened for

4

selective activity against the CSCs. The model consists of HMLE control cells and HMLE cells with knocked-down E-cadherin (HMLEshEcad), which display characteristics of cancer stem cells, such as: mesenchymal phenotype, ability to form mammospheres, $CD44^{high}/CD24^{low}$ marker profile, resistance to chemotherapeutic drugs and others [3].

As said, it was demonstrated that CSCs possess an enhanced ROS defense capability compared to their non-stem cell counterparts. Therefore, strategies to abrogate ROS defense in CSCs or the discovery of non-toxic molecules that selectively upregulate ROS in malignant cells might result in the eradication of these ROS-resistant cells and thereby provide a basis for the development of efficient cancer therapies [4,5].

The lack of significant progress in the CSC-targeted treatments reveals the need for new therapeutic approaches, such as photodynamic therapy (PDT). PDT has been investigated as a promising alternative non-invasive method for cancer treatment [6]. The method is based on the sensitization of oxygen to the singlet excited state by dyes [7]. Compounds that are mostly used in the treatment are sensitizers with porphyrine structure [8]. However, a progress has been made recently in the use of nanoparticles [9]. Indeed, nanomedicine has great potential in the development of CSC-targeting drugs, controlled drug delivery and release, and the design of novel gene-specific drugs and diagnostic modalities [10]. Nevertheless, for the further development of the clinical method and search for new targets and compound *leads*, it is of pivotal importance to find new phototherapy mechanisms and get their full understanding on molecular level. One promising group of the phototherapeutic agents are quinone methides (QMs), reactive intermediates encountered in the chemistry and photochemistry of phenols [11]. It is widely accepted that biological action of QMs stems from their reactivity with DNA, since antineoplastic antibiotics such as mitomycin exhibit antiproliferative action on metabolic

formation of QMs and subsequent alkylation of DNA [12,13,14,15,16]. However, QMs react with other biologically relevant nucleophiles, and particularly with amino acids [17] and proteins [18]. We have recently demonstrated that antiproliferative activity of photogenerated QMs stems from their reaction with intracellular proteins rather than with DNA [19].

QMs can be formed under mild conditions in photochemical reactions [14,15], such as photodeamination from the Mannich salts of the corresponding phenols [17,20], particularly applicable to biological systems [21,22]. Moreover, photodehydration of hydroxybenzyl alcohols [23], is a convenient method for the QM generation. Although dehydration takes place less efficiently then the elimination of ammonium salts, it is more appealing due to the fact that the thermal back-hydration regenerates the starting material, so there is no loss of an active molecule inside the cell due to the competing reaction of a QM with H_2O. In addition to simple phenol derivatives [23], the photodehydration has been demonstrated on naphthols [24], or anthrol derivatives [25,26]. Adequately substituted anthrols **1** can be excited with near visible light at $\lambda >$ 400 nm delivering **QM1** in photodehydration or photodeamination [26]. The QMs react with nucleophiles giving adducts. Preliminary biological investigation indicated enhancement of antiproliferative activity for the human cancer cells which were irradiated, suggesting that the effect is due to intracellular photochemical formation of QMs [25,26].

Dichotomy of photochemical pathways leading to QMs or singlet oxygen generation has recently been described as a function the QM-precursor substituents by Freccero *et al.* [27], but their biological effects were not evaluated. Herein we perform a detailed photochemical and photobiological investigation on a series of anthracene derivatives **2**-**5**. The molecules were strategically designed to probe for the effect of molecular structure to biological effect. Whereas

excitation of **2** can give QMs, **3**-**5** cannot undergo photodehydration and deliver QM. Furthermore, **2** and **3** can both give phenoxyl radicals in the photochemical reaction, but **4** and **5** cannot. The highest yield of singlet oxygen formation is anticipated from anthracene derivative **4** without strong electron donating substituent. Phenoxyl radicals and singlet oxygen are anticipated to lead to oxidative stress. Freccero *et al.* demonstrated phototoxicity of Mannich bases due to the generation of reactive phenoxyl radicals [28]. Photochemical reactivity of **2**-**4** has been investigated by performing preparative irradiations in the de-aerated and aerated solutions where the differences are expected for molecules that can sensitize oxygen. In addition, irradiations of **2** have been conducted in the presence of nucleophiles to demonstrate the ability of photochemically formed QMs to give adducts. Photophysical properties were investigated by fluorescence spectroscopy, whereas formation of QM, phenoxyl radicals and other potential reactive intermediates that could result in biological effects was probed by laser flash photolysis (LFP).

Biological investigations included antiproliferative assessment of four human cancer cell lines, HCT 116 (colon), MCF-7, SUM 159 (breast), H 460 (lung). We additionally used a breast epithelial stem-like cell model described above [3], in order to test their potential CSC-selectivity. The cells were kept in dark or irradiated. Interestingly, all anthracene derivatives **2**-**4** showed enhanced antiproliferative activity on exposure to irradiation. We additionally tried to explain their biological effects, demonstrate their localization within the cells and also validate their selectivity.
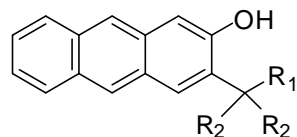
1a R_1 = OH, R_2 = CH$_3$
1b R_1 = OH, R_2 = Ph
1c R_1 = N(CH$_2$CH$_3$)$_2$, R_2 = H
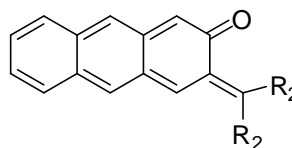
QM1a R_2 = CH$_3$
QM1b R_2 = Ph
QM2 R_2 = H
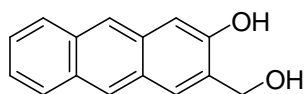
2
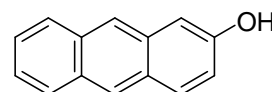
3
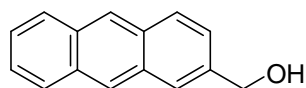
4
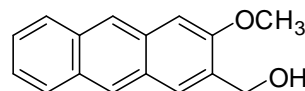
5

Results

Synthesis and photochemistry

Anthrols **1** and **3** were prepared according to the described procedures, whereas **4** can be purchased. Synthesis of anthrol **2** was accomplished in five steps, starting from the commercially available 2-aminoanthraquinone which was converted to carbaldehyde **6** following the procedure in literature precedent [26]. Reduction of the aldehyde with NaBH$_4$ afforded anthrol **2** in almost quantitative yield (Scheme 1).
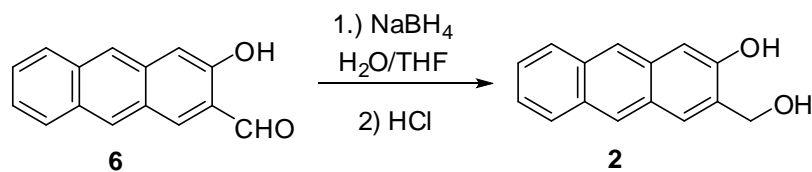
Scheme 1. Synthesis of **2**.

Synthesis of methoxy derivative **5** started from aldehyde **6** which was methylated to methyl ether **7**, and then reduced to afford **5** in excellent yield (Scheme 2).

8

6 → **7** → **5**
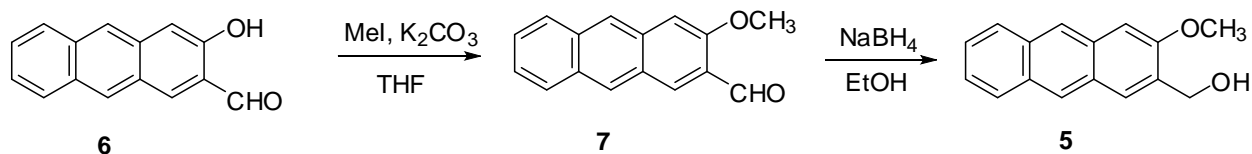
Scheme 2. Synthesis of anthryl methyl ether **5**.

Based on literature precedent [23,25], it is expected that irradiation of **2** in CH_3OH-H_2O gives rise to photomethanolysis products *via* a QM intermediate. Preparative irradiations of **2** were conducted by irradiating CH_3OH-H_2O (4:1) solutions at 350 nm and by analyzing the composition of the solutions by HPLC. Methanolysis of **2** run to the conversion of 80% gave cleanly methyl ether **8** (Scheme 3). Photomethanolysis was also conducted by irradiating **2** in CH_3OH-H_2O (4:1) by use of lamps with the output at 420 nm or visible light where the same product **8** was obtained (see Fig S1 in the supporting info). The finding is important for the applicability of anthracene **2** in biological media where 350 nm irradiation can excite intracellular molecules, whereas 420 nm or visible light is harmless.

2 → **8**
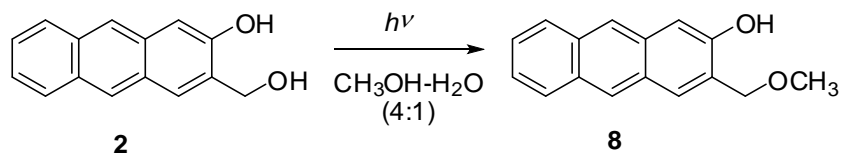
Scheme 3. Photomethanolysis of **2**.

The efficiency of the photomethanolysis (Φ_R) for **2** was investigated by simultaneous use of three actinometers, ferrioxalate ($\Phi_{254} = 1.25$) [29,30], KI/KIO$_3$ ($\Phi_{254} = 0.74$) [29,31], and valerophenone ($\Phi_{254} = 0.65 \pm 0.03$) [29,32] as it was described for the determination of the Φ_R for **1b** ($\Phi_R = 0.023 \pm 0.001$) [25]. The measured value of Φ_R determined by use of three actinometers for **2** is $\Phi_R = 0.22 \pm 0.01$. Interestingly, ten times higher value of Φ_R was obtained for nonsubstituted **2**, then for phenyl-substituted **1b**. On the contrary, biphenyls or phenols

bearing phenyl at the hydroxymethyl group react more efficiently then the corresponding nonsubstituted derivatives [14].

Importance of the free phenolic OH in the methanolysis was demonstrated by irradiating methyl ether **5** in CH_3OH-H_2O (4:1), under the same conditions as **2**, wherein **5** remained unchanged. Furthermore, irradiation of **2** in CH_3OH, gave higher yields of **8** at higher H_2O concentration (see Fig S2 in the supporting info), in accordance with the faster phenol deprotonation from S_1 to H_2O-clusters then to CH_3OH [33,34].

To show that **QM2** is an intermediate in the photochemistry of **2**, irradiation was performed in CH_3CN solution in the presence of other nucleophiles, ethanolamine, and sodium azide, ubiquitous quencher of QMs [14,20,25], as well as with ethyl vinyl ether (EVE) which is known to react with QMs in a Diels-Alder reactions [35]. Whereas photolyses in the presence of ethanolamine and EVE did not give any new product, azide adduct **9** was isolated in 30% yield. The lack of reactivity with ethanolamine may be ascribed to its basicity. Thus, ethanolamine deprotonated anthrol **2** and decreased efficiency for the QM formation, as reported for **1** [25]. On the contrary, EVE probably did not affect QM formation, but the adduct was not formed due to too short lifetime of **QM2** (*vide infra*) and too low rate constant for the Diels-Alder reaction [20,25].
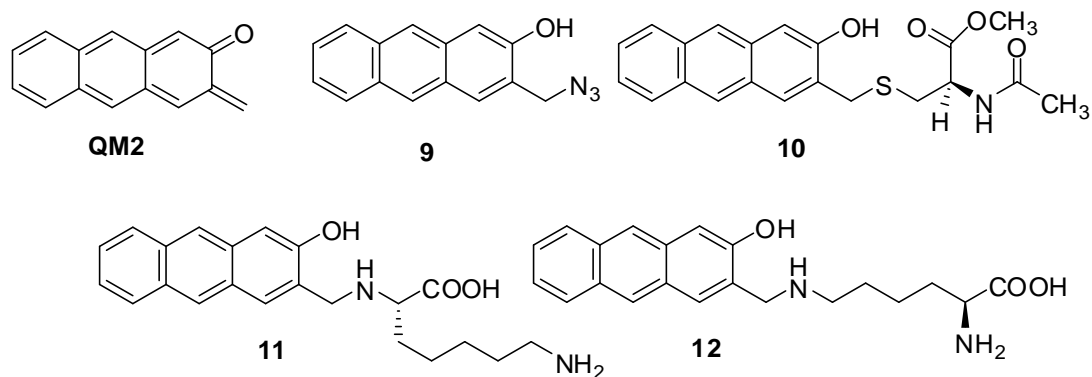
To demonstrate the ability of **QM2** to react with amino acids and induce alkylation of proteins, irradiation of **2** was conducted in the presence of lysine and N,C-protected cysteine **13**. Photolysis of **2** (5×10^{-4} M in CH_3CN-H_2O 9:1) in the presence of cysteine **13** (5×10^{-2} M) gave one new product **10** (65% in 20 min irradiation at 350 nm using 8 lamps with the 8 W output), whereas in the presence of lysine two products were detected by HPLC and potentially assigned to **11** and **12**. Due to small quantities of photoproducts, it was more convenient to synthesize them then to isolate them from the photochemical mixtures. Synthesis of **10** started from anthracene **2** which was acetylated and treated with trimethylsilyliodide (TMSI) [36] formed *in situ*, to afford iodide **15** (Scheme 4). The reaction of **15** with the protected cysteine derivative **13** in the presence of diisopropylethylamine, and subsequent acetyl hydrolysis under basic conditions gave **10** which was isolated and fully characterized. Comparison of the HPLC chromatograms of **10** and the photolysis mixture after irradiation of **2** in the presence of the protected cysteine undoubtedly showed that **10** was formed in the photochemical reaction (see Fig S3 in the supporting information).
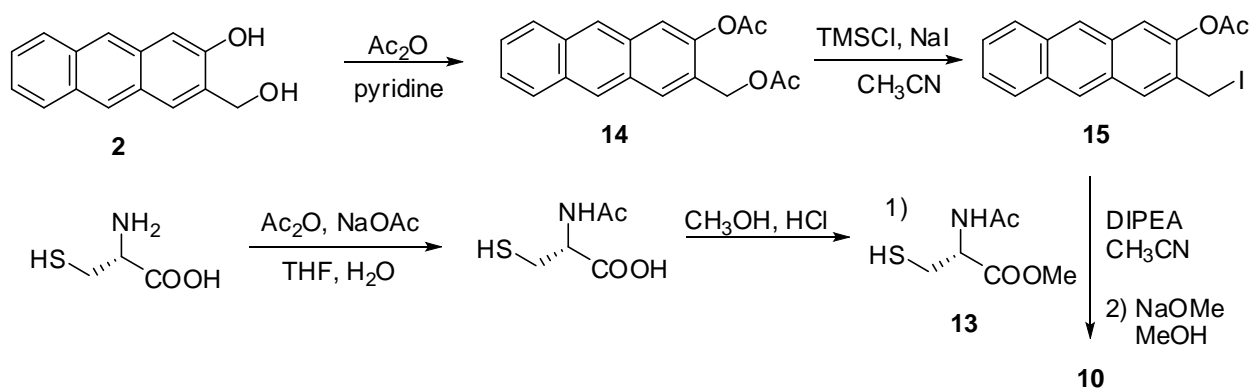
Scheme 4. Synthesis of photoproduct **10**.

A mixture of adducts **11** and **12** was prepared from aldehyde **6** which was in the presence of L-lysine transformed to the Schiff bases, and *in situ* reduced with sodium borohydride to afford the lysine adducts (Scheme 5). Unfortunately, the compounds were highly insoluble in all solvents which precluded their purification and full characterization.
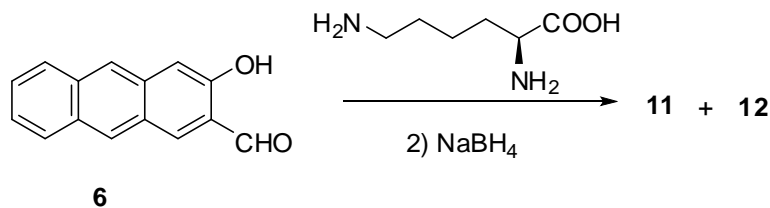
Scheme 5.

Particularly relevant to the biological systems is the photochemical reactivity of **2**-**4** in aerated solutions. To probe for the reactivity in the presence of oxygen, photolyses of **2** were conducted in CH_3CN or CH_3CN-H_2O in UV-vis cells where solutions were not purged with N_2 or Ar prior to the irradiation. After each exposure to 350 nm light, UV-vis spectra were recorded (see Figs S4 and S5 in the SI). After the irradiation, new bands appeared in the spectra at 420-500 nm, which after several hours did not disappear, indicating formation of stable oxidation products. To isolate oxidation products, irradiations of **2**-**4** were conducted in O_2-saturated CH_3CN-H_2O solutions. Irradiations gave products **16**-**18**, respectively, which were fully characterized (Schemes 6-8). Evidently, in the presence of oxygen, anthracenes were photooxidized. Anthrol derivatives **2** and **3** underwent oxidation at the anthracene positions 1 and 2, whereas hydroxymethyl anthracene was oxidized at positions 9 and 10 giving derivatives of 1,2- or 9,10-anthraquinone, respectively. Most probably, anthracene in the excited state sensitizes formation of singlet oxygen that oxidizes molecules.
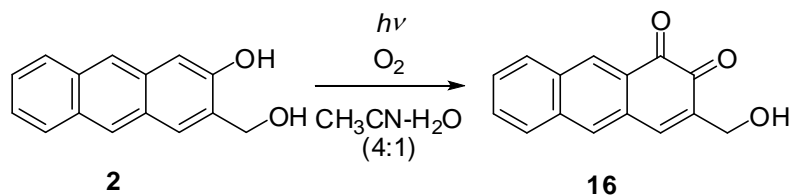
Scheme 6.
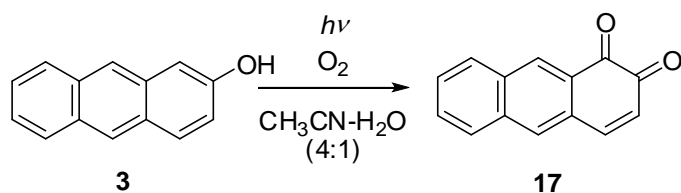
Scheme 7.
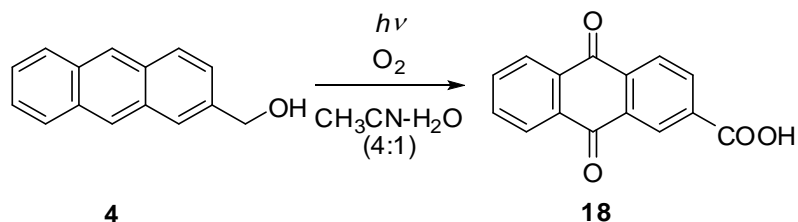
Scheme 8.

Photophysical properties, binding to protein and DNA

Fluorescent properties of **2**-**4** are important for the understanding of their photochemical reactivity from S_1, as well as for the potential applications in fluorescent microscopy. Fluorescence spectra for **2**, **3** and **5** were measured in CH_3CN, and CH_3CN-H_2O (1:1) (For the absorption and fluorescence spectra see Figs S6-S11 in the supporting information). The absorption spectra of **2**, **3** and **5** in CH_3CN are characterized with a band at 310-420, corresponding to $S_0{\rightarrow}S_1$ transition. Compared to the absorption spectrum of **4**, those of anthrol derivatives **2**, **3** and **5** are batochromically shifted $\approx$50 nm, which enables excitation of molecules with near-visible light (>400 nm), particularly important for biological applications.

13

Fluorescence spectra of **2**, **3** and **5** in CH_3CN have bands at 400-450 nm, and the quantum yields are very high, $\Phi_F = 0.7$-0.9 (Table 1). Decay of fluorescence was fit to monoexponential function with relatively long S_1 lifetimes ($\tau = 17$-25 ns).

Addition of H_2O to the CH_3CN solution significantly quenched fluorescence for **2** and **3**, but not for **5** which does not have free phenolic OH (for the quenching plot of **2** see Fig S8 in the supporting information). In addition, in aqueous solution for **2** and **3**, the typical dual fluorescence was observed due to the emission of phenol (400-500 nm) and phenolate (500-600 nm) formed in S_1 by excited state proton transfer (ESPT) to solvent. ESPT was also indicated by single photon counting (SPC), where bi- or triexponential function was used to fit the decays with rising components (negative pre-exponential factor) for the traces collected at longer wavelengths. All data obtained by steady-state and time-resolved fluorescence are consistent with ESPT reactivity of **1**-**3** in aqueous solution giving phenolates. Moreover, for **1** and **2** (compounds that can give QMs) the best fit was obtained with three-exponential function and two negative pre-exponential factors. The result indicates that phenolate is formed with different rate constants from two fluorescent phenol species. Smaller Φ_F in aqueous solution for **1b** and **2**, compared to **3**, and three-exponential decays indicate additional photochemical deactivation channel from S_1 for anthrols **1b** and **2**, not taking place with **3**, most probably formation of QMs.

Table 1. Photophysical properties of anthracenes **1b**, **2**, **3** and **5**.

	$\Phi_F(CH_3CN)$[b]	$\Phi_F(CH_3CN-H_2O)$[b]	τ (CH_3CN)/ns [c]	τ (CH_3CN-H_2O)/ns [c]
1b[a]	0.86 ± 0.01	0.39 ± 0.01	17.8 ± 0.1	1.8 ± 0.2
				8.1 ± 0.2
				24.5 ± 0.1 phenolate
2	0.73 ± 0.03	0.33 ± 0.01	24.9 ± 0.2	≈ 0.1
				8.60 ± 0.01
				20.8 ± 0.1 phenolate
3[a]	0.88 ± 0.05	0.57 ± 0.02	25.3 ± 0.1	15.4 ± 0.1 phenol
				25.3 ± 0.1 phenolate
5	0.90 ± 0.05	0.85 ± 0.05	25.1 ± 0.1	28.4 ± 0.1

[a] Taken from ref [25]. [b] Quantum yields of fluorescence (Φ_F) were measured by use of quinine sulfate in 0.05 M aqueous H_2SO_4 ($\Phi_F = 0.53$) as a reference.[29] [c] Singlet excited state lifetimes and decay times were obtained by global fitting of fluorescence decays measured by time-corrected single photon counting. The quoted error corresponds to the maximum absolute deviations.

Ability of anthrol **2** to bind to proteins (bovine serum albumin, BSA) and DNA was essayed by UV-vis and fluorescence spectroscopy. The measurements were performed in CH_3CN-H_2O (1:9) in the presence of phosphate buffer (pH = 7, c = 1 mM). Due to high lipophilicity, **2** probably aggregates in the solution at high water content, which was indicated from the UV-vis spectra by the increased absorbance at 413 nm at the low energy edge of the spectrum (compared to CH_3CN). On addition of **2** to the solution of BSA (see Figs S12-S14 in the supporting information), the band at 413 nm in the absorption spectrum decreased intensity relatively to the band at 257 nm. The observation suggests that **2** binds to the protein, whereupon it probably deaggregates. Fluorescence spectra further supported binding of **2** to BSA. When the solution of **2** was added to BSA, the fluorescence (λ_{ex} = 295 nm) of BSA was quenched, whereas fluorescence of **2** increased compared to the solution of **2** without BSA. The quenching of BSA fluorescence is probably due to FRET from tryptophan to **2** (see fig S12 in the supporting information). Moreover, upon excitation at λ > 350 nm, where only **2** absorbs, addition of BSA

15

resulted in the batochromic shift (≈10 nm) of the fluorescence spectrum, and changed the relative ratio of the phenol and phenolate emission, suggesting that **2** is bound to less hydrophilic environment in the protein where it is less deprotonated then in H_2O. Upon irradiation of **2** in the presence of protein (420 nm) the fluorescence decreased, suggesting reaction with the protein. However, attempts to detect adducts of **QM2** with protein by MALDI failed, probably due to a small increase of m/z compared to the protein molecular weight.

Contrary to the noncovalent binding to BSA, preliminary investigation by UV-vis and fluorescence spectroscopy suggested that **2** does not bind to ct-DNA, or that the binding constant is small (see Figs S15 and S16 in the supporting information). In the presence of DNA, no changes in the UV-vis spectra were detected, whereas the fluorescence was weakly quenched ≈10% (upon excitation at 390 nm where only anthracene absorbs light, see Fig S15 in the SI). Due to aggregation of **2** in the aqueous solution, determination of the binding isotherms with BSA or DNA was precluded. However, upon irradiation (420 nm) of **2** in the presence of DNA, significant fluorescence quenching was observed, presumably due to covalent binding to DNA. Spectroscopic investigation for **2** in the presence of BSA and DNA indicates significant noncovalent interactions with the protein, but noncovalent binding to DNA is probably weak. However, upon irradiation of **2**, photochemically generated **QM2** can probably alkylate both, DNA and protein.

Laser Flash Photolysis (LFP)

LFP experiments were conducted for molecules **2**, **3** and **5** to probe for QMs and other reactive intermediates that could interact with biologically important molecules, with the excitation at 355 nm by the use of a Nd:YAG laser. The transient absorption spectra were measured in

CH$_3$CN and CH$_3$CN-H$_2$O, where difference was anticipated due to ESPT pathways. Moreover, the measurements were conducted in N$_2$- and O$_2$-purged solutions, where O$_2$ is expected to quench some transient species (triplets and radicals), but QMs and carbocations should not be affected.

The transient absorption spectra for **2** in CH$_3$CN and CH$_3$CN-H$_2$O are shown in Fig 1, whereas for other spectra and quenching plots see supporting information Figs S17-S28.
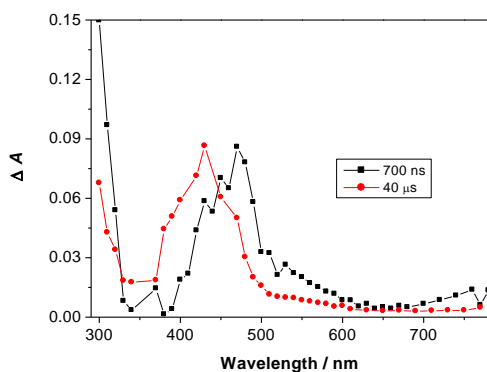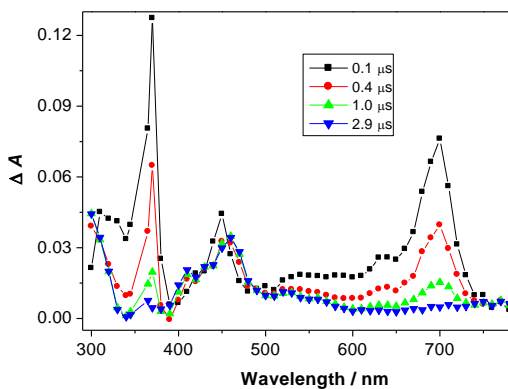
Fig 1. Transient absorption spectra in O$_2$ purged and optically matched ($A_{355} \approx 0.40$) solutions of **2** in CH$_3$CN (top) and CH$_3$CN-H$_2$O (1:1) bottom.

In both N_2- and O_2-purged CH_3CN solution of **2**, a transient was detected with a maximum at 690 nm that decayed to a baseline with unimolecular kinetics (N_2-purged solution, $k = 1.67 \times 10^6$ s^{-1}, $\tau = 590 \pm 10$ ns; O_2-purged solution, $k = 2.3 \times 10^6$ s^{-1}). The transient was quenched with CH_3OH ($k_q = 5.6 \times 10^6$ $M^{-1}s^{-1}$) or H_2O, but the rate constant for the quenching by H_2O could not be revealed since the Stern-Volmer plot is not linear (See Figs S20 in the SI). Thus, in aqueous solution, the transient at 700 nm is very short-lived with $\tau \approx 20$ ns, at the detection limits of the setup used. Based on the comparison with precedent spectra [37,38] and quenching with nucleophile CH_3OH, the transient at 700 nm was assigned to radical-cation **19**. It is formed in a monophotonic process, since the intensity of the transient depends linearly on the laser power (see Fig S16 in the supporting information). In the aqueous solution, the phenol radical-cations deprotonate giving phenoxyl radicals [39], which may explain non-linear quenching of the transient by H_2O, as seen in the systems undergoing ESPT [40].
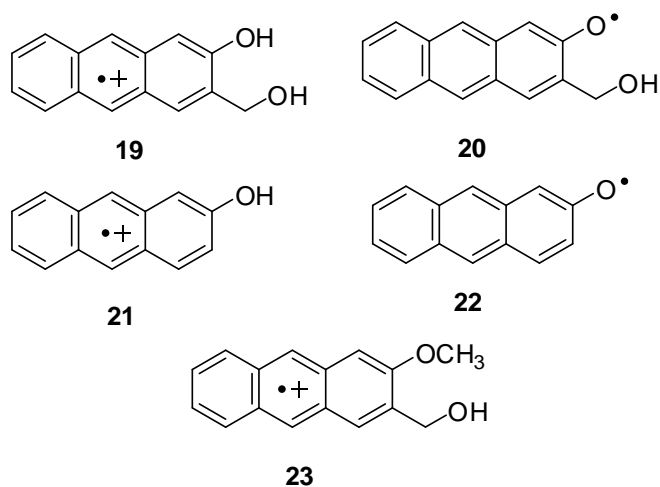
In aqueous O_2-purged solution of **2**, several transient species were detected, a faster decaying transient at 400-600 nm ($\tau = 15 \pm 1$ μs), whose decay matched the rise of a more persistent transient absorbing at shorter wavelength 300-400 nm (see Fig S22 in the supporting

information), decaying slower over ms timescale. Even though we used the modified LFP setup without a lamp pulser [41], precise decay kinetics for the long-lived transient could not be revealed due to low transient intensity and long lifetime over which the lamp intensity fluctuated. The short-lived transient (τ = 15 μs) was tentatively assigned to phenoxyl radical **20**, based on the position of the absorption maximum and decay kinetics from precedent literature [26,42,43]. For the long-lived transient, we propose it corresponds to **QM2**, based on literature precedent [26]. It is probably formed by the homolytic cleavage of the OH group from phenoxyl radical **20**, since the kinetics of its formation corresponds to the decay of **20**. However, due to low intensity of the transient assigned to **QM2**, quenching experiments that would prove the assignment were precluded.

LFP experiments for **2** were also conducted in 2,2,2-trifluoroethanol (TFE), a polar non-nucleophilic solvent in which electrophilic species such as QMs [44] and carbocations [45,46] exhibit particularly long lifetimes (see Fig S24 in the supporting information). Contrary to **1a**, we have got similar transient absorption spectra in TFE and CH_3CN-H_2O.

LFP experiments for **3** in CH_3CN (see Fig S25 in the supporting information) revealed formation of radical-cation **21**, absorbing at 700 nm (N_2-purged solution, $k = 4.75\times10^5$ s^{-1}, τ = 2.1±0.1 μs). In the aqueous solution **21** could not be detected since it deprotonates to phenoxyl radical **22** absorbing at 400-550 nm, decaying with slower kinetics ($k = 3.3\times10^4$ s^{-1}, τ = 30±10 μs). Methoxy derivative **5** undergoes one photon ionization to radical-cation **23**, absorbing at 700 nm (see Figs S27-S29 in the supporting information). Since **23** cannot deprotonate, it has a longer lifetime and similar decay kinetics in both CH_3CN and CH_3CN-H_2O (O_2-purged CH_3CN-H_2O, $k = 4.7\times10^4$ s^{-1}, τ = 20±1 μs). Thus, phenoxyl radical from **5** cannot be formed, so after the decay of **23** no other long-lived transients were detected.

The results obtained by LFP experiments with **3** and **5** additionally corroborate the assignments of the observed transient for **2**, at 700 nm to radical-cations, and 400-500 nm to phenoxyl radicals (only seen for **2** and **3**). The detection of phenoxyl radicals **20** and **22** is important for biological systems since it is expected that these intermediates interact with biologically important molecules such as proteins and DNA, as well as to interact with reactive oxygen species (ROS) formed by sensitization, or that are naturally present in the cell.

Biology

Antiproliferative tests

In a preliminary study of antiproliferative investigation of **1** on three human cancer cell lines, HCT 116 (colon), MCF-7 (breast), and H 460 (lung), with and without exposure to irradiation (350 and 420 nm) we showed that the exposure of the cells treated with **1** to irradiation induced a higher cytotoxic effect than cells that were kept in the dark [25,26]. This suggests that the enhanced antiproliferative activity is due to the photogeneration of QMs. In the here-presented study we assessed the antiproliferative activity of **2**-**4** on the same cell model (Table 2). It can be seen that the exposure of cells treated with tested anthracenes to irradiation induced a higher cytotoxic effect than cells that were kept in the dark, except for MCF-7 cells treated with **4** that induced similar or even stronger effect without the irradiation. For the irradiation, fluorescent lamps were used with the emission at 320-400 nm (the maximum at ≈350 nm), or with the emission at 380-450 nm (the maximum at ≈420 nm). The irradiation of cells incubated with **1**-**3** at 420 nm induced somewhat stronger cytotoxic effect than at 350 nm, while the irradiation of cells treated with **4** at 350 nm induced a more pronounced effect, which is in accordance with the absorption spectrum of **4** overlapping with the emission of the lamps.

In general, the most apparent enhancement of antiproliferative activity is induced by the irradiation of anthracene **2**. Furthermore, as already mentioned in the introduction, we have been especially interested in the activity of tested compounds on cell lines that display characteristics of cancer stem cells, such as mesenchymal phenotype, ability to form mammospheres, $CD44^{high}/CD24^{low}$ marker profile, resistance to chemotherapeutic drugs and others. Therefore, we additionally tested compounds **1b** and **24** on SUM 159, representing basal breast cancer cell line with high proportion of $CD44^{high}/CD24^{low}$ cells [47], as well as on a breast epithelial stem-like cell model obtained from the Dr. R. Weinberg laboratory [3]. This model consists of HMLE control cells (HMLEshGFP) and HMLE cells with knocked-down E-cadherin (HMLEshEcad), which display characteristics of stem cells, such as mesenchymal morphology, $CD44^{high}/CD24^{low}$ antigen profile and an increased resistance to the chemotherapeutic drug paclitaxel, which we confirmed (Supporting information Figure S29). Interestingly, although in general similar effect of activity enhancement by irradiation was noticed on these cell lines, it can be noted that HMLE cell lines were more sensitive towards **1b** and **2** compared to other cell lines, whereby modest or no enhancement of antiproliferative activity was noticed after the irradiation of cells incubated with **1b**.

Also, it can be seen that SUM 159 cells were generally more sensitive to treatments compared to MCF-7 cells, while the difference between HMLEshGFP and HMLEshEcad was less obvious, except for compound **4**. Although the irradiation at 350 nm produced more pronounced effect of compounds **1b** and **2**-**3**, compared to 420 nm, at the same time the irradiation of control, non-treated cells at 350 nm was shown to be especially harmful for SUM 159 and HMLEshEcad cells. Therefore, we decided to proceed with other experiments using 420 nm light, which was

harmless for the cells. These lamps are an ideal excitation source for **1b** and **2**-**3**, and can be used to excite compound **4**, although less efficiently.

Table 4. IC$_{50}$ values (μM)[a], obtained by MTT test.

Cell line	compound / treatment	1b	2	3	4
HCT116	Not irradiated	21±0.3	≥100	27±17	>100
	350nm 3×5 min	2±0.4	2±0.2	9±8	1±0.1
	420nm 3×5 min	2±0.4	1±0.4	2±0.1	2±0.8
H 460	Not irradiated	19±1	≥100	23±5	33±15
	350nm 3×5 min	3±1	15±6	12±2	1±0.1
	420nm 3×5 min	2±0.2	10±3	2±0.5	2±0.9
MCF-7	Not irradiated	20±0.5	≥100	28±9	0.1±0.1
	350nm 3×5 min	4±3	2±0.7	2±0.7	0.5±0.2
	420nm 3×5 min	2±0.1	3±1	1±0.5	2±0.1
SUM159	Not irradiated	4±2	11±8	18±2	13±5
	350nm 3×5 min	-	-	-	-
	420nm 3×5 min	1±1	2±0.3	2±1	1±0.4
HMLEshGFP	Not irradiated	6±4	11±3	27±8	33±8
	350nm 3×5 min	1±0.6	0.7±0.7	2±0.05	0.6±0.2
	420nm 3×5 min	2±0.02	1±0.4	2±0.1	10±0.1
HMLEshEcad	Not irradiated	2±0.5	17±13	25±2	22±13
	350nm 3×5 min	2±0.3	2±0.3	2±0.05	1±0.4
	420nm 3×5 min	2±0.3	1±1	1±0.2	2±0.1

[a] Concentration that causes 50% inhibition of the cell growth.

A
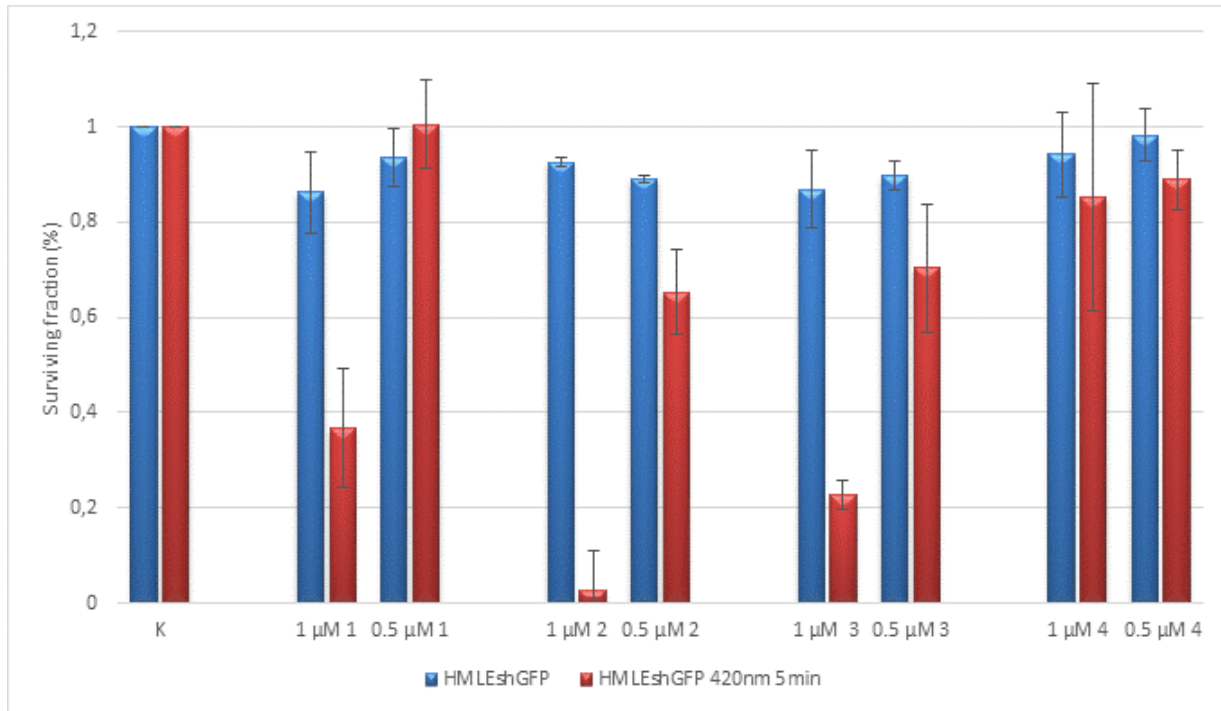
B
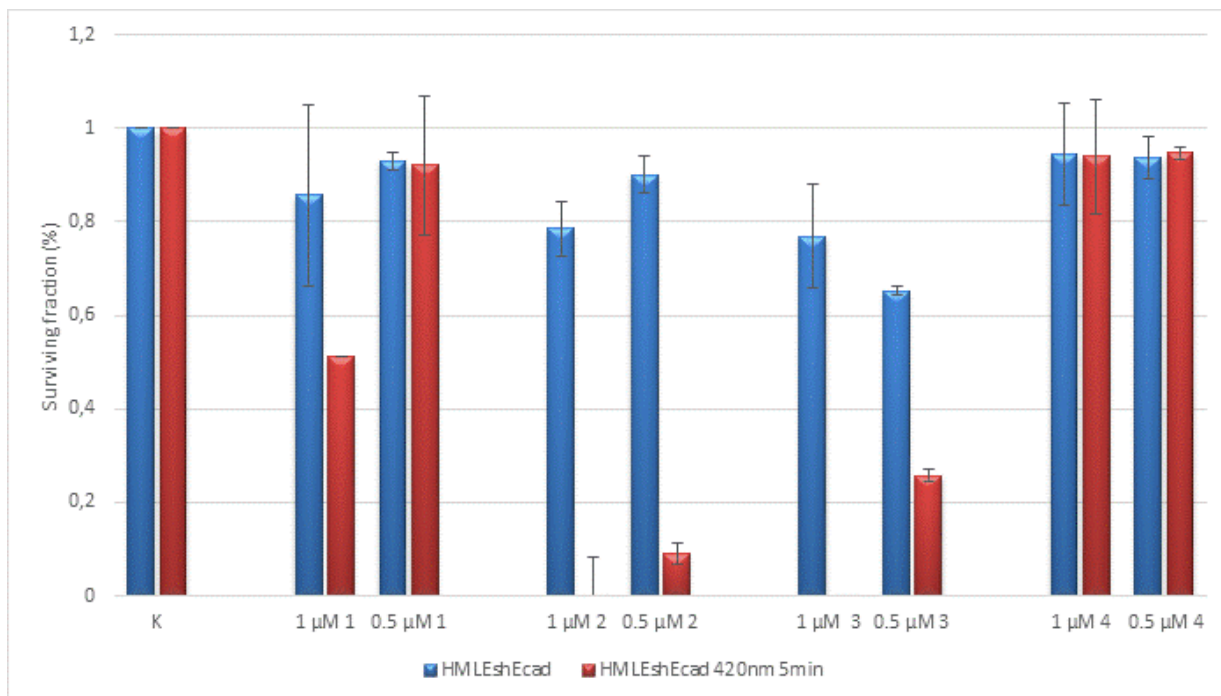
Figure 2. Clonogenic assay performed on HMLEshGFP (a) and HMLEshEcad (b) cells treated with **1b** and **2** - **4** (1 µM and 0.5 µM) for 24 h. Cells HMLEshGFP 420 nm 5min and HMLEshEcad 420 nm 5 min were additionally irradiated four hours upon the addition of the compounds with 420 nm for 5 min. SF – surviving fraction. Error bar represents standard deviation of at least three independent experiments.

Since MTT test allows for the detection of antiproliferative effect in relatively short time (72 hours), we decided to perform the clonogenic (or colony forming) assay. It measures the capacity of cells to produce progeny (a single cell to form a colony of 50 or more cells) between control untreated cells; i.e. it measures a long-term effect of tested compounds and is commonly used for monitoring the efficacy of radiation modifying compounds and for determining the effects of anti-cancer therapeutics on colony forming ability in cell lines. We used concentrations that were close or slightly lower to the IC_{50} obtained after the irradiation of cells (1 µM and 0.5 µM).

In accordance with the results obtained by MTT assay, it is evident that the activity of compounds **1b** and **2**-**3** is substantially enhanced after the irradiation, mostly for **2** and **3** (Figure 2). On the other side, the activity of compound **4** was negligible and not enhanced upon irradiation. The reason for this is the combination of relatively low compound concentration and the excitation wavelength (420 nm), not matching the absorption spectrum of compound **4**. Besides, it should be noted that the cells were irradiated three times during MTT assay, while just once for the clonogenic assay.

Importantly, the inhibition of colony formation of HMLEshEcad cells upon irradiation of compounds **2** and **3** (at both tested concentrations) was significantly more pronounced in comparison to HMLEshGFP cells, pointing to a potential selective inhibitory effect towards

tumor stem-like cells. Treatment with compound **1b** at 1 µM, along with the irradiation significantly, but comparably inhibited both cell lines.

Cell cycle experiments

In order to get further insight into the potential mechanism of activity of tested compounds, we assessed their influence on the cell cycle of HMLEshEcad and HMLEshGFP, as well as MCF-7 and SUM159 cells, 24 and 48 hours after the treatment with compounds with or without the irradiation of cells (Figure 3 and 4 and data not shown). The results show that the treatment with **1b** and **2** without the irradiation did not significantly influence the cell cycle of HMLEshGFP and HMLEshEcad cells, except that higher concentration of **1b** induced G1 delay in HMLEshGFP cells. However, the irradiation of the treated cells induced a delay in S/G2 phase, whereby both compounds caused the most pronounced effect at the 5 µM concentration. What's more, the influence of compounds was more pronounced on HMLEshEcad cells.

Contrary to the effect of **1b** and **2**, compounds **3** and **4** did influence the cell cycle to some extent even without the irradiation, by inducing the G1/S delay in HMLEshEcad cells (Figure 4). Irradiation of treated cells, on the other side, induced the accumulation of cells in S and G2/M phases, whereby the effect of compound **4** on HMLEshGFP is significantly less obvious than on HMLEshEcad. This effect is still present after 48 h of treatment (data not shown). However, a pronounced cytotoxic effect (a high percent of dead cells) is also obvious, especially after the treatment with higher compound concentration.

Similar strong cytotoxic effect was observed after the treatment of MCF-7 and SUM159 cells, but without any meaningful effect on the cell cycle (data not shown).

In conclusion, although compounds do induce particular effects on the cell cycle of HMLE cells, which are different and/or more pronounced after the irradiation, they are not straightforward and do not unambiguously point to a specific mechanism of activity. Rather, the compounds induce a strong cytotoxic effect.
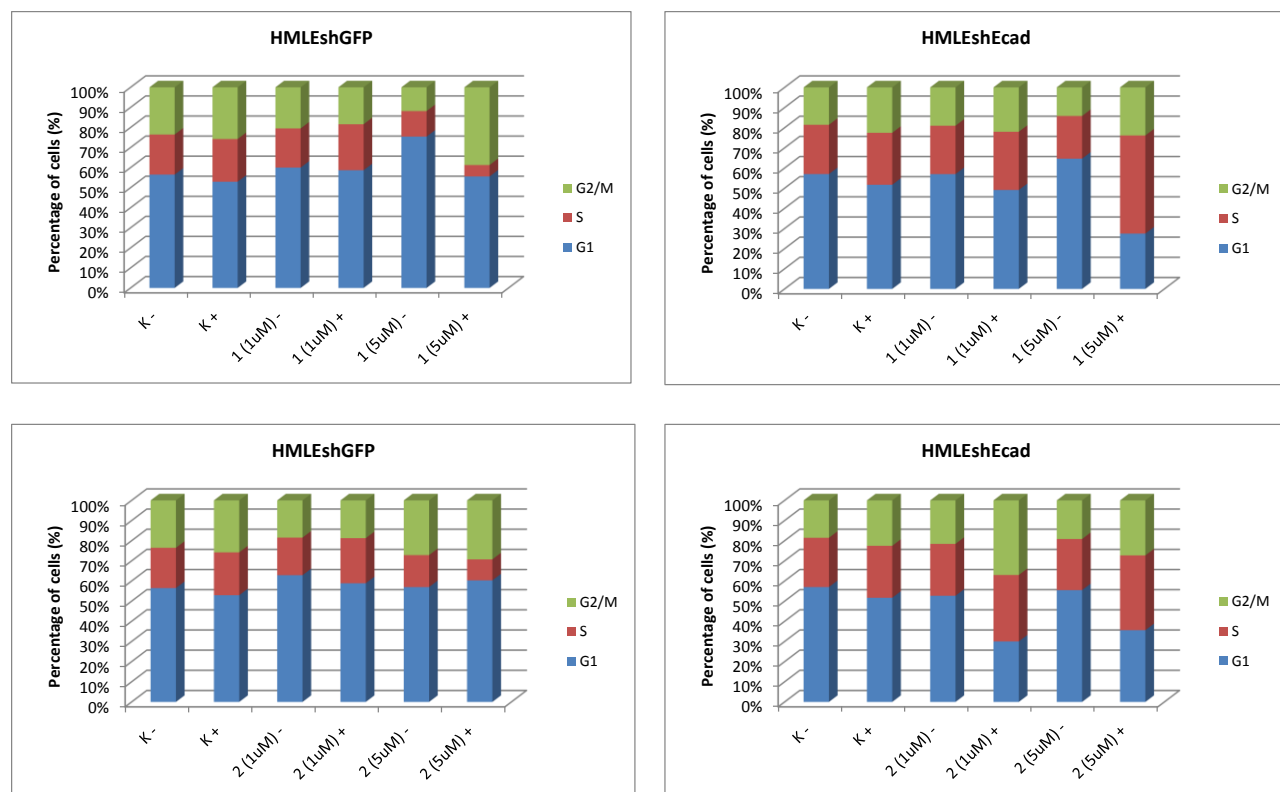
Figure 3. The effect of compounds **1b** and **2** at 1 μM and 5 μM concentrations on the cell cycle distribution of HMLEshGFP and HMLEshEcad cells after 24 h treatments with (+) or without (-) the irradiation at 420 nm/5 min. The histograms represent the percentage of cells in the respective cell cycle phase (G1, S and G2/M), obtained by flow cytometry. K - = non treated and not irradiated cells; K+ = non treated, irradiated.
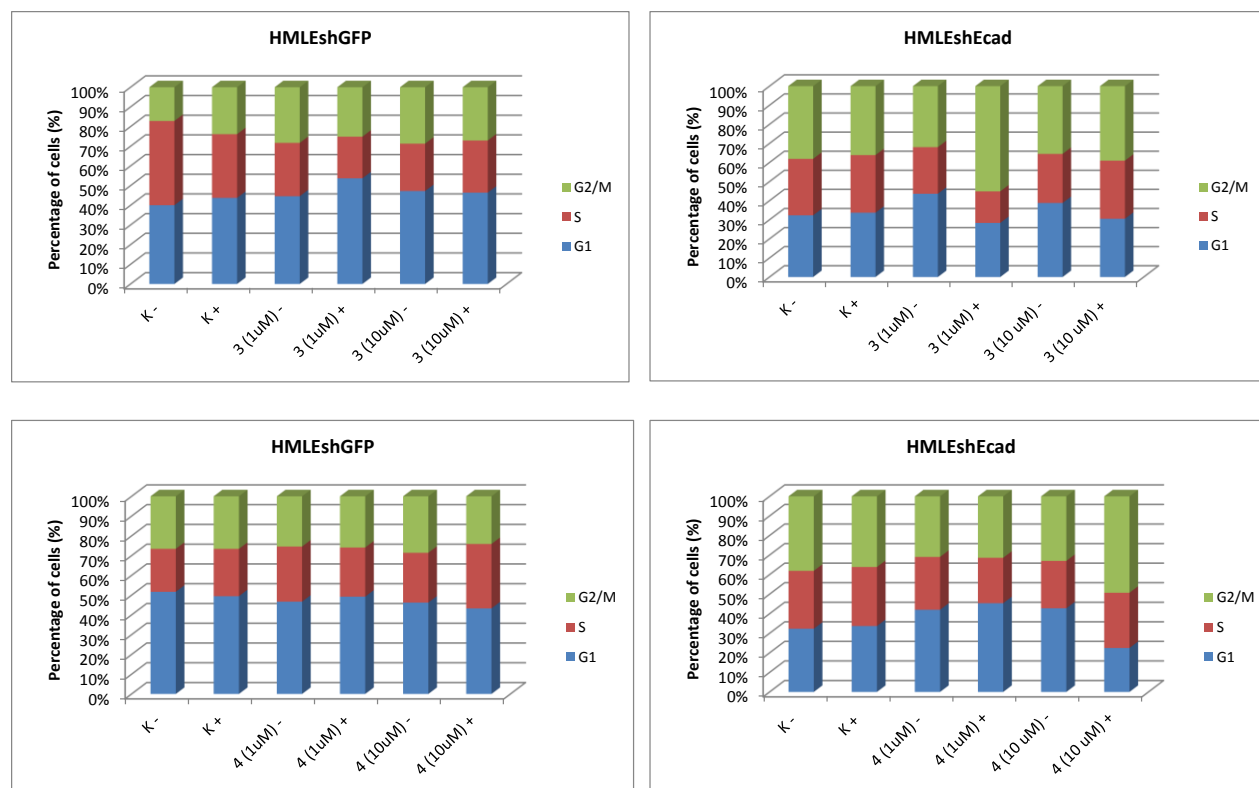
Figure 4. The effect of compounds **3** and **4** at 1 μM and 10 μM concentrations on the cell cycle distribution of HMLEshGFP and HMLEshEcad cells after 24 h treatments with (+) or without (-) the irradiation at 420 nm/5 min. The histograms represent the percentage of cells in the respective cell cycle phase (G1, S and G2/M), obtained by flow cytometry. K - = non treated and not irradiated cells; K+ = non treated, irradiated.

Assessment of cellular ROS levels following treatment with 3 and 4

Since we previously found that anthracenes **2**-**4** sensitize formation of singlet oxygen that oxidizes molecules, we tested if the enhanced effect of **3** and **4** upon irradiation could be ascribed to the formation of reactive oxygen species (ROS). We measured the intracellular ROS levels

28

using H2DCFDA in SUM159, MCF-7, HMLEshEcad and HMLEshGFP cells. A slight induction of ROS was detected in SUM159 cells treated with **3** and irradiated, while no difference was noticed in MCF-7 cells (supporting information, Figure S30). On the other hand, a significantly elevated level of ROS was detected in HMLEshGFP cells after treatment with both compounds at 1 µM and 10 µM concentrations and upon subsequent irradiation of cells (Figure 5): a 2-fold induction after treatment with **3** at both concentrations and a 4-fold induction after the treatment with **4** at 10 µM. Importantly, HMLEshEcad cell line was even more susceptible to ROS induction compared to HMLEshGFP cells, whereby the irradiation of HMLEshEcad cells treated with **4** at 10 µM induced a 7-fold increase of ROS levels compared to non-irradiated cells (Figure 5).

In contrast to this, the treatment of HMLEshEcad cells with **3** at lower concentrations, without the irradiation, demonstrated even a slight decrease in the intracellular ROS levels compared to the control cells, which suggests that this compound has intrinsically antioxidative capacity (Supporting information, Figure S31). Antioxidative activity of some phenols such as resveratrol has been demonstrated [48].
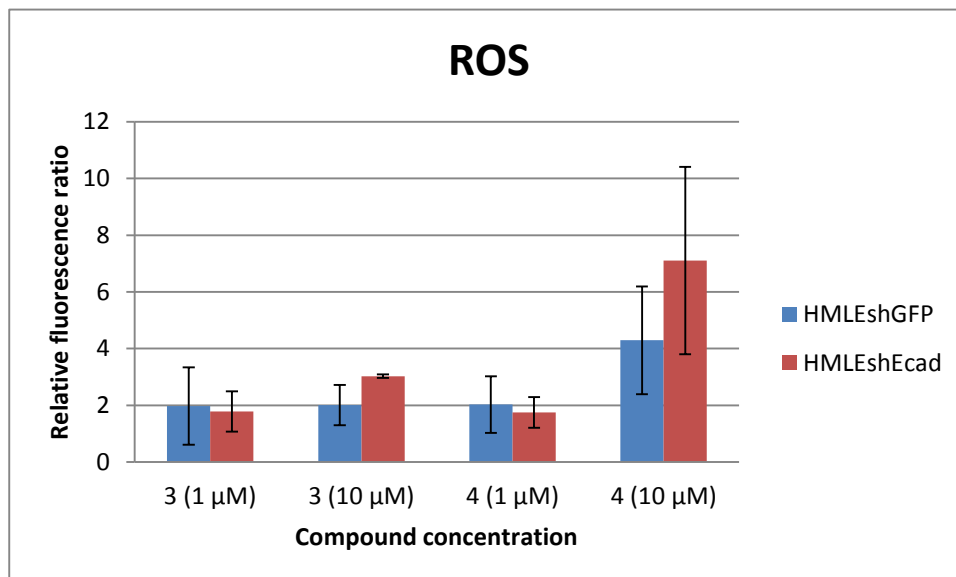
Figure 5. Detection of ROS levels using H2DCF-DA dye by FACS analysis. HMLEshEcad and HMLEshGFP cells were treated with **3** or **4** (1 μM and 10 μM) and irradiated for 5 min, 420 nm. Results are shown as ratios of mean fluorescence of treated and irradiated cells to irradiated control cells *vs.* treated and non-irradiated cells to non-irradiated controls (means ± SD from three independent experiments).

Intracellular localization of compounds in living cells

To check the intracellular distribution of the compounds, HMLEshGFP and HMLEshEcad cells were incubated for 3 h with the tested compounds and confocal laser scanning microscopy was used. For illumination, the 405 nm laser line was used to excite compounds **1b**, **2** and **3** and fluorescence emission was detected in the 440 - 560 nm range. Compound **4** cannot be excited with monochromatic 405 nm, so we could not detect its emission/localization. However, when UV-light was used for the excitation of **4**, its fluorescence was detected inside the cells, and it was evident only in the cytoplasm, but not in the nucleus (data not shown). The preliminary

experiments showed that the cellular distribution of tested compounds was comparable in both cell lines.

The results made evident that none of the compounds localized in the nucleus, but were predominantly distributed throughout the cytoplasm, where, upon the irradiation react with and bind to both plasma and intracellular membranes (Figures 6 - 8 and S33-S35). This is demonstrated by an intense reticular fluorescence pattern in the cytoplasm, as well as on the plasma membrane. Certain, but small differences can be observed between the localization of the three compounds.

For example, compound **1b** additionally formed noticeable aggregates, which could suggest its aggregation due to high lipophilicity and/or its localization in lysosomes or endosomes (Figure 6). Interestingly, a formation of distinct spherical protrusions (i.e. blebs) could be observed on the cells' surface, obviously as a result of cell exposure to stress. Since no evidence of cytoplasmic material could be observed within the blebs, they do not point to apoptotic, but most probably to necrotic cell death [49,50]. What is more, in case the cells were irradiated for 5 min (420 nm) three h after the addition of **1b**, incubated in freshly prepared compound and then subjected to confocal microscopy, the cellular damage was even more severe (Figure 7). More intense fluorescence was evident in perinuclear region and plasma membrane, indicating cell swelling (necrotic volume increase), uncoupling of the cytoskeleton from the plasma membrane and degradation of the internal structure of the cell (Figure 7). As demonstrated previously, necrotic blebs form in cells exposed to more intense noxious stimuli such as hypoxia, metabolic poisoning and high concentrations of free radicals [50].
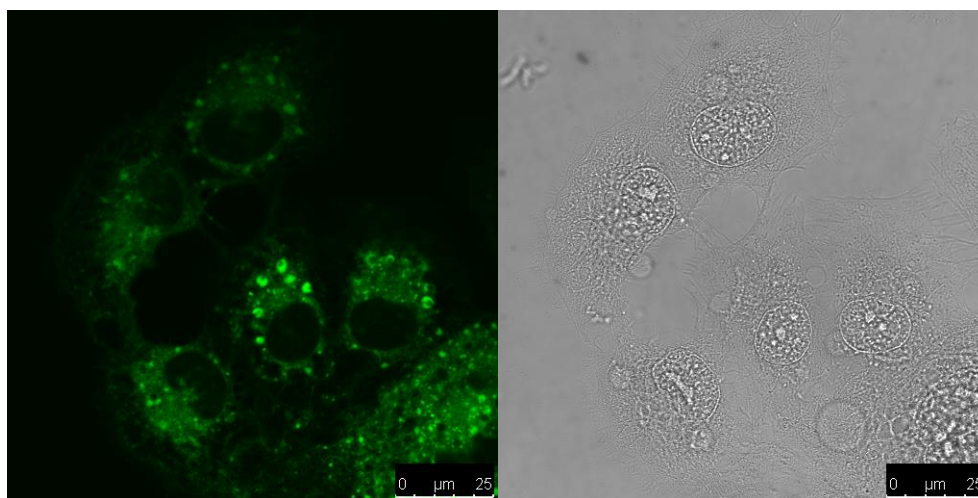
Figure 6. Confocal microscopy image of HMLEshEcad cells. Left panel - the fluorescence images, excitation at $\lambda_{\mathrm{ex}} = 405$ nm and detection at 440 - 460 nm; right panel – the same images in the transmitted light. The cells were treated for 3 h with compound **1b** (5 µM), rinsed and analyzed by confocal microscopy.
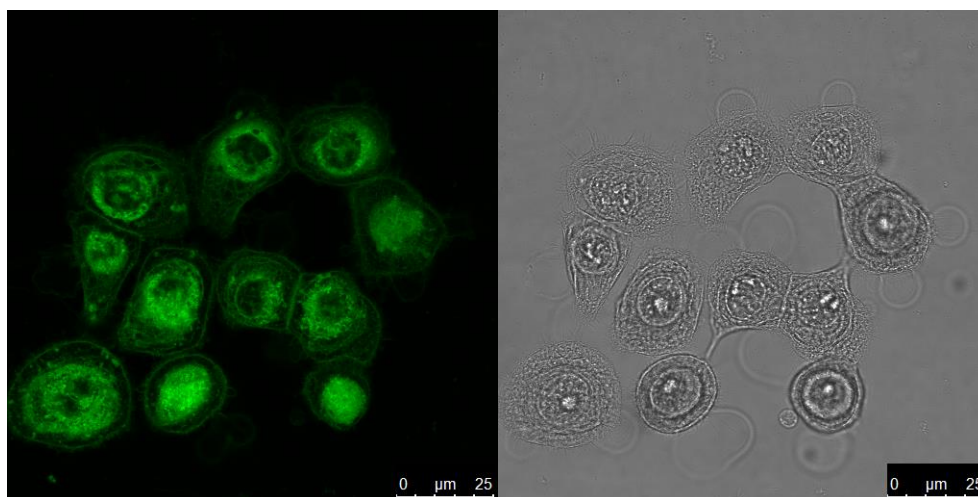
Figure 7. Confocal microscopy image of HMLEshGFP cells. Left panel - the fluorescence images, excitation at $\lambda_{\mathrm{ex}} = 405$ nm and detection at 440 - 460 nm; right panel – the same images in the transmitted light. The cells were treated for 3 h with compound

1b (5 µM), irradiated for 5 min at 420 nm. The cells were then incubated in freshly prepared compound dilution, rinsed and analyzed by confocal microscopy.

Similar, somewhat more diffuse localization pattern was observed for compound **2**, which was localized more distinctively in perinuclear region, pointing to a possible colocalization with endoplasmic reticulum (ER) or Golgi apparatus (Figures 8 and S33). Also, upon additional irradiation for 5 min before the microscopy, distinctive perinuclear aggregates could be observed (Figure 8).
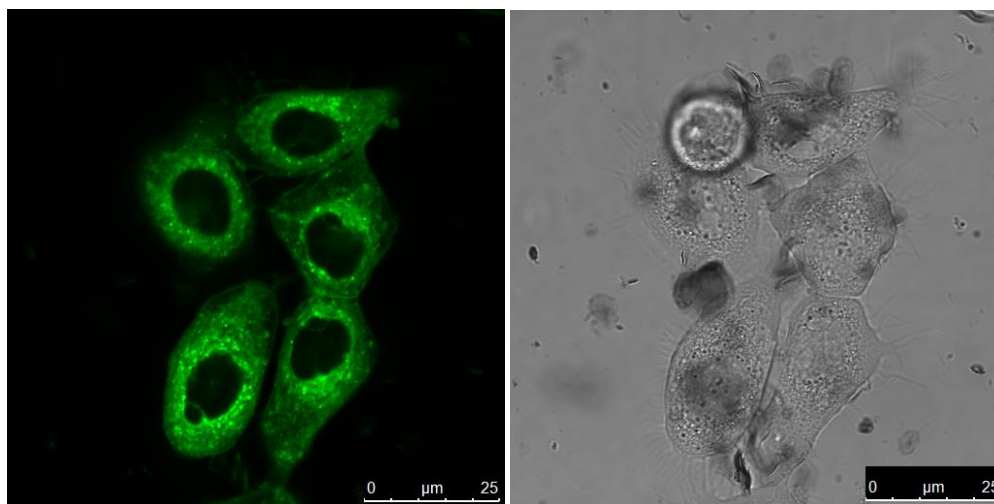
Figure 8. Confocal microscopy image of HMLEshGFP cells. Left panel - the fluorescence images, excitation at λ_{ex} = 405 and detection at 440 - 460 nm; right panel – the same images in the transmitted light. The cells were treated for 3 h with compound **2** (5 µM), irradiated for 5 min at 420 nm. The cells were then incubated in freshly prepared compound dilution, rinsed and analysed by confocal microscopy.

Similarly, compound **3** did not enter the nucleus, but is predominantly distributed throughout the cytoplasm (Figure S34 and S35). This is demonstrated by an intense fluorescence pattern in the cytoplasm, mostly in the perinuclear region. Also, the treatment of cells with **3** resulted in excessive cell membrane blebbing, followed by cell swelling and degradation (Figure S35).

In conclusion, the here-presented results unequivocally confirm that all tested compounds cannot enter the nucleus and consequently cannot react with DNA. On the other hand, they predominantly react with cell membranes, however further experiments should be performed in order to confirm their exact localization. Nevertheless, the presented results encourage further study of these compounds as potential fluorescent markers for cell membranes.

Discussion

Cancer stem cells (CSCs) are a minor subpopulation of cancer cells that share properties of embryonic stem cells like pluripotency and self-renewal. They also appear to be involved in cell migration, invasion, metastasis, and treatment resistance, all of which lead to poor clinical outcomes [2]. Therefore, targeting CSCs, rather than cancer cells in general, is a novel and highly promising strategy for cancer treatment. A variety of therapeutic approaches to inhibiting CSC-related pathways are currently being tested in preclinical and clinical trials. Still, as a result of current treatments failing to target CSCs, novel therapies such as photodynamic therapy (PDT) are being investigated [51].

PDT involves the treatment of cancer cells with an inactive and nontoxic photosensitizer (PS), which is activated by light with specific wavelength, matching its absorbance. Numerous studies demonstrated that PDT initiates a cascade of chemical reactions, involving ROS production, which trigger apoptosis, necrosis, and autophagy of cells [6]. Further development of cancer treatment approaches and search for new targets and compound leads, requires discovery and elucidation of novel phototherapy mechanisms on molecular level. It is widely accepted that the choice of the sensitizers and the type of their interaction with the target cells are most essential

34

factors in the success of PDT. What is more, one of the key aspects of this interaction is the subcellular localization of the PS and the precise way that PDT influences cellular pathways is largely governed by PS localization. The subcellular localization in turn is governed by the chemical nature of the PS, such as molecular weight, lipophilicity, ionic charge, protein binding characteristics, etc. For example, PS can localize in mitochondria, lysosomes, endoplasmic reticulum, Golgi apparatus and plasma membranes [52,53]. It is therefore important to confirm the target biomolecules and select the appropriate sensitizers relevant for tumor therapy. Interaction and damaging of biological macromolecules became interesting approach in different cancer therapies [54].

A promising group of phototherapeutic agents are reactive intermediates - quinone methides (QMs). It is well established that QMs react with biologically important molecules, typically with nucleic acids, but also with amino acids and proteins, particularly with cysteine residues [18]. One of the methods for the generation of QMs is photodehydration or phototautomerization of phenol derivatives.

The objective of the research described herein was to investigate photochemical reactivity of anthracene derivatives **1b** and **2**-**4** and correlate it with the anticancer potential in dark and upon the irradiation. The molecules are particularly interesting in biology since they can be excited with near visible light at $\lambda > 400$ nm. It should be noted, however, that for the real cancer phototherapy molecules that absorb at $\lambda > 600$ nm should be designed. We have demonstrated that photoexcitation of **1b** and **2** leads to the dehydration and QM formation that were detected by LFP. QMs react with good nucleophiles such as azide and thiols, as well as moderately strong nucleophile CH_3OH. Adducts with nucleophiles were isolated in the preparative irradiation experiments. However, short QM lifetime impedes the Diels-Alder reactions, reported in the

naphthalene series [55]. On the other hand, **3** and **4** cannot undergo photodehydration, but lead to the formation of phenoxyl radical or singlet oxygen, as demonstrated by LFP or isolation of oxidized products, respectively. Particularly appealing property of anthrols **1b** and **2**-**3** is their high fluorescent quantum yield, enabling their localization in cells in the biological experiments. Furthermore, compound **2** binds non-covalently to BSA, whereupon it senses the change of media polarity, leading to the different emission, and probably, to the alkylation of the protein. Therefore anthrol **2** has a potential to be used as a fluorescent label in biology.

All compounds moderately inhibited cell proliferation without the irradiation, except compound **4**, which showed significant cytotoxicity only toward MCF-7 cells. Although upon the irradiation of cell lines treated with **1b** and **2**-**4**, an enhancement of antiproliferative activity was demonstrated to various extends, the DNA is not the target biomolecule, i.e. the DNA damage is not a potential mode of their activity. This was confirmed by confocal microscopy study, which showed that none of the tested compounds entered the nucleus, as well as by UV-vis and fluorescence spectroscopy that confirmed that **2** did not non-covalently bind to ct-DNA. On the other hand, all compounds localize and react with various cellular membranes, whereupon photochemical excitation they can induce damage of the membranes, or surrounding proteins. Similar distribution pattern was already described for some PS [56]. Although mitochondria seem to play a major role in photodynamic cell death, lysosomes were also proposed to be a critical intracellular target. However, it was shown that the relative efficacy was lower, probably due to the tendency of PS with greater degrees of aggregation to accumulate in lysosomes [52]. Our results also point to potential aggregation and accumulation of **1** in lysosomes. On the other hand, compound **2** was localized more distinctively in perinuclear region, pointing to a possible colocalization with ER or Golgi apparatus.

Special attention of our study was put to demonstrate the potential selectivity of these compounds towards the cells with CSC-like properties. We used a model cell line in which epithelial-to-mesenchymal transition (EMT) is induced by knocking-down E-cadherin (HMLEshEcad), and which was shown to result in the enrichment of cells with stem-like properties [3]. We also tested the compounds on two breast cancer cell lines, which differ in the proportion of cells with characteristic stem cell markers ($CD44^{high}$/$CD24^{lo}$), i.e. MCF-7 (low proportion), and SUM 159 (high proportion). Although SUM 159 cells were generally more sensitive to all compounds compared to MCF-7 without the irradiation, the additional irradiation resulted in comparable cytotoxicity, measured by MTT assay. Interestingly, compound **2** demonstrated enhanced activity towards cancer stem-like cells (HMLEshEcad) in clonogenic assay, compared to their control counterparts (HMLEshGFP). Although the underlying mechanism is not clear, it might be related to its localization in ER/Golgi apparatus, since the ER was shown to be an "Achille's heel" of cells that had undergone EMT [57].

All cell lines were comparably sensitive to **3** in both tests. Unfortunately, a slightly enhanced activity of **4** towards HMLEshEcad cells, obtained in MTT was not confirmed in clonogenic assay, probably because of an inappropriate wavelength of light and only one irradiation dose, as well as a low concentration of compound **4**. Still, we were especially interested in the ability and/or selectivity of compounds **3** and **4** to induce ROS upon irradiation in tested cells. Namely, the use of PDT as a cancer therapy is particularly attractive because of its dual selectivity: the precise focus of the light on the tumor and the specific subcellular localization of PS in malignant cells. Exactly why cells die, or whether there are particular cellular macromolecules that are more susceptible to oxidation by singlet oxygen or other PDT-generated ROS has been the subject of many investigations [53]. Redox dysregulation represents a specific weakness

associated with many tumors and results in activation of multiple cell death pathways. In spite of the fact that excess ROS could produce toxic off-target effects, evidence show that unacceptable off-target effects and systemic toxicity can be avoided by adjusting the treatment according to tumors' alterations in redox signaling, metabolic profile or other specific tumor vulnerabilities [58]. Also, the type of ROS generated, the location of its generation, as well as the local concentration is important for the cellular functions of ROS in cancer cells. A challenge for novel therapeutic strategies will be the fine tuning of intracellular ROS signaling and the discovery of non-toxic molecules that selectively upregulate ROS in malignant cells, resistant to therapy. Of note, among many putative mechanisms of resistance of cancer stem cells towards therapy, the enhanced ROS scavenging is a very important one [59,60].

In our study, we also detected lower basal levels of ROS in control (HMLEshGFP) cells, compared to CSC-like cells (HMLEshEcad) (Figure S32). However, our results demonstrated that both **3** and **4** induced ROS in this cell model, whereby **4** at 10 μM concentration induced even higher levels of ROS in CSC-like cells, in spite of imperfect light source. Although being very preliminary, these results are especially encouraging, and point toward a further investigation of the exact localization of this compound, specific type of ROS generated in the cells, as well as further cell death signaling mechanism, which all should elucidate the underlying mechanism of the observed selectivity. Thus far, our results indicate that necrosis is a dominant cell death mechanism. Necrosis is caused by physical or chemical damage and has generally been considered an unprogrammed process. It is characterized by cytoplasm swelling, destruction of organelles and disruption of the plasma membrane, leading to the release of intracellular contents and inflammation [53]. The crucial factors in determining the type of cell death, e.g. apoptosis or necrosis, following PDT are cell type, the subcellular localization of the

PS and the light dose applied to activate it. In general, it is believed that lower dose PDT leads to apoptosis, while higher doses lead to proportionately more necrosis. And generally, necrosis and autophagy may be dominant cell death modes after PDT when apoptosis is dysfunctional. However, since PS may localize in more than one organelle, as we demonstrated in our study, the activation of various cell death pathways may occur concurrently [61].

Conclusion

In summary, this study evaluated a photochemical and photobiological characterization of anthrol derivatives **1b** and **2**-**4** and their anticancer potential. We demonstrated that upon the irradiation with near visible light at $\lambda > 400$ nm **1b**-**2** can give QMs, while **3**-**4** cannot undergo photodehydration and deliver QM, but lead to the singlet oxygen formation. Special attention was put to demonstrate the potential selectivity of these compounds towards the cells with CSC-like properties. Although the excitation wavelength used in our study, is not desirable for PDT (it should be >600 nm, in order to penetrate the organs more deeply and have less side effects), we demonstrated the proof-of-concept that the anthrols can be used as lead compounds for PDT. Firstly, with an adequate molecular design, these compounds could be tuned to either generate ROS, or QMs, as an alternative mechanism of PDT. Secondly, these compounds enter the cell and, upon irradiation react with cellular membranes. This finding points toward further study of their precise subcellular localization. This, in turn will enable either their development of potential membrane/organelle fluorescent markers, or photosensitizers with particular subcellular localization (primarily ER and Golgi apparatus), which consequently induce specific mode of cell killing and/or potential selectivity towards resistant cells. Finally, our preliminary

experiments demonstrate an intriguing cytotoxic activity of anthrols, and selectivity of both **2** and **4** towards CSC-like cell model. Especially interesting is the selectivity of **4** that produced higher levels of ROS in CSC-like cells. This result forms the basis for further research on cancer phototherapy, as well as for the elucidation of CSC selectivity based on oxidative stress activation.

Experimental

General information

^{1}H and ^{13}C NMR spectra were recorded at 300, or 600 MHz at rt using TMS as a reference and chemical shifts were reported in ppm. Melting points were determined using a Mikroheiztisch apparatus and were not corrected. IR spectra were recorded on a spectrophotometer in KBr and the characteristic peak values were given in cm^{-1}. HRMS were obtained on a MALDI TOF/TOF instrument. For the sample analysis a HPLC was used with C18 (1.8 μm, 4.6×50 mm) column. HPLC runs were conducted at rt (~25 °C) and chromatograms were recorded using UV detector at 254 nm. For the chromatographic separations silica gel (0.05–0.2mm) was used. Irradiation experiments were performed in a reactor equipped with 8 or 12 lamps (1 lamp, 8 W) with the output at 350 nm. During the irradiations, the irradiated solutions were continuously purged with Ar and cooled by a tap-water finger-condenser. Solvents for irradiations were of HPLC purity. 3-Hydroxyanthracene-2-carbaldehyde (**6**) was prepared according to literature precedant [26] starting from commercially available 2-aminoanthraquinone [25]. Chemicals were purchased from the usual commercial sources and were used as received. Solvents for chromatographic

separations were used as they are delivered from supplier (p.a. grade) or purified by distillation (CH_2Cl_2).

3-Hydroxmethyl-2-hydroxyanthracene (2)

Aldehyde **6** (175 mg, 0.71 mmol) was suspended in CH_3OH-THF (1:1, 20 mL) and $NaBH_4$ was added under inert atmosphere (N_2). The reaction mixture was stirred overnight at rt, whereupon the color changed from orange to pale yellow and a precipitate was formed. Water (20 mL) was added dropwise, followed by the adition of 1M HCl until pH~3 was achieved. The stirring was continued for 15 min, and the product was filtered off. The product was washed with a large amount of water until neutral pH of the filtrate was achieved, then dried in an evacuated dessicator over KOH. Pure product **2** (155 mg, 98 %) was obtained in the form of yellowish powder.

3-Hydroxmethyl-2-hydroxyanthracene (2): 155 mg (98 %); m.p. 228-230 °C; ^{1}H NMR (300 MHz, DMSO-d_6) δ/ppm: 10.0 (br. s, 1H), 8.42 (s, 1H), 8.24 (s, 1H), 8.00-7.93 (m+s, 2H+1H), 7.46-7.32 (m, 2H), 7.21 (s, 1H), 5.70 (br. s, 1H), 4.68 (s, 2H); ^{13}C NMR (150 MHz, DMSO-d_6) δ/ppm: 153.2 (s), 133.7 (s), 132.0 (s), 131.3 (s), 129.4 (s), 128.0 (d), 127.4 (s), 127.3 (d), 125.4 (d), 125.1 (d), 125.0 (d), 123.9 (d), 122.3 (d), 105.9 (d), 58.8 (d); IR (KBr) $\tilde{v}$/cm^{-1}: 3448 (s), 3182 (m), 2930 (w), 1699 (s), 1447 (m), 1244 (w), 1213 (m), 1005 (m), 893 (m), 737 (s), 474 (m); HRMS-MALDI calcd. for $C_{15}H_{12}O_2$ (-e$^-$) 224.0832, found 224.0830.

3-Methoxyanthracene-2-carbaldehyde (7)

Aldehyde **6** (100 mg, 0.45 mmol), K_2CO_3 (200 mg, 1.45 mmol) and MeI (100 μL, 1.61 mmol) were dissolved in dry THF (10 mL) and the resulting suspension was heated on reflux overnight.

The solvent was removed on a rotary evaporator and the solid residue was extracted with CH_2Cl_2 (3×15 mL). After the filtration, the solvent was removed on a rotary evaporator. The crude product was purified on column of silica gel using CH_2Cl_2 as an eluent. Product **7** (64 mg, 60 %) was obtained in the form of yellow crystalline solid.

3-Methoxyanthracene-2-carbaldehyde (**7**): 64 mg (60 %); ^{1}H NMR (300 MHz, CDCl$_3$) δ/ppm: 10.6 (s, 1H), 8.53 (s, 1H), 8.47 (s, 1H), 8.23 (s, 1H), 7.99-7.88 (m, 2H), 7.53-7.38 (m, 2H), 7.23 (s, 1H), 4.04 (s, 3H); ^{13}C NMR (75 MHz, CDCl$_3$) δ/ppm: 190.0 (d), 156.1 (s), 134.0 (s), 133.7 (s), 132.6 (d), 130.7 (s), 129.6 (d), 128.4 (d), 127.4 (d), 126.9 (d), 126.6 (s), 124.9 (d), 124.0 (d), 104.3 (d), 55.4 (q).

3-Hydroxymethyl-2-methoxyanthracene (**5**)

In a round bottom flask (25 mL) aldehyde **7** (50 mg, 0.21 mmol) was suspended in EtOH (10 mL). Under inert atmosphere (N_2) NaBH$_4$ (20 mg, 0.53 mmol) was added. The yellow suspension immediately become clear and the color changed to pale yellow. The resulting mixture was stirred 1 h at rt. The solvent was removed on a rotary evaporator and the resulting solid residue was suspended in water (15 mL). The product was extracted with CH_2Cl_2 (5×15 mL), the combined extracts were dried over anhydrous MgSO$_4$, filtered and the solvent was removed on a rotary evaporator. Product **5** (42 mg, 84%) was obtained in the form of yellowish solid.

3-Hydroxymethyl-2-methoxyanthracene (**5**): 42 mg (84 %); m.p. 150-152 °C; ^{1}H NMR (300 MHz, CDCl$_3$) δ/ppm: 8.25 (s, 1H), 7.95 (s, 1H), 7.94 (t, 2H, $J = 9.4$ Hz), 7.86 (s, 1H), 7.46-7.38 (m, 2H), 7.19 (s, 1H), 4.85 (s, 2H), 3.99 (s, 3H); ^{13}C NMR (150 MHz, CDCl$_3$) δ/ppm: 155.7 (s), 132.2 (s), 132.0 (s), 131.6 (s), 130.5 (s), 128.1 (d), 127.9 (s), 127.5 (d), 126.1 (d), 125.4 (d),

124.4 (d), 123.8 (d), 103.5 (d), 62.5 (t), 55.3 (q); IR (KBr) $\tilde{v}$/cm^{-1}: 3281 (m), 2862 (w), 1637 (m), 1466 (m), 1273 (w), 1217 (s), 1009 (m), 905 (m), 739 (m), 473 (m); HRMS-MALDI calcd. for C$_{16}$H$_{14}$O$_2$ (-e$^-$) 238.0990, found 238.0992.

Preparative photochemical methanolysis

Irradiation of 3-hydroxymethyl-2-hydroxyanthracene (**2**). Compound **2** (15 mg, 0.067 mmol) was dissolved in methanol (80 mL) in a quartz vessel, and water (20 mL) was added. The resulting solution was purged with a stream of Ar (20 min), and irradiated in a Rayonet reactor using 12 lamps at 350 nm for 15 min. Prior to and during the irradiation, the solution was continuously purged with a stream of Ar and cooled using a coldfinger condenser. The reaction was monitored by HPLC and the irradiation was stopped when ~80 % conversion to the photoproduct was achieved. The solvent was removed on a rotary evaporator and the crude product was purified on short column of silica gel using CH$_2$Cl$_2$ as an eluent to give product **8** (13 mg, 80%) of in the form of pale yellow film.

3-Methoxymethyl-2-hydoxyanthracene (**8**) [26]: 13 mg (80 %); m.p. 189-192 °C; ^{1}H NMR (300 MHz, CDCl$_3$) δ/ppm: 8.29 (s, 1H), 8.22 (s, 1H), 7.95-7.88 (m, 2H), 7.73 (s, 1H), 7.45-7.37 (m, 2H), 7.36 (s, 1H), 4.84 (s, 2H), 3.50 (s, 3H); ^{13}C NMR (75 MHz, CDCl$_3$) δ/ppm: 153.5 (s), 132.8 (s), 132.2 (s), 130.3 (s), 128.2 (d), 128.0 (d), 127.7 (d), 126.2 (s), 126.1 (d), 125.5 (d), 124.4 (d), 123.8 (d), 109.3 (d), 74.2 (t), 58.2 (q); IR (KBr) $\tilde{v}$/cm^{-1}: 3228 (m), 2928 (m), 1637 (s), 1445 (m), 1213 (m), 1076 (m), 887 (s), 737 (m), 473 (m).

3-Azidomethyl-2-hydroxyanthacene (**9**)

Compound **2** (15 mg, 0.067 mmol) was dissolved in acetonitrile (70 mL) and the solution of NaN$_3$ (1 g, 15 mmol) in water (30 mL) was added. Photolysis was carried out in a Rayonet reactor using 11 lamps at 350 nm for 30 min. Prior to and during the irradiation, the solution was continuously purged with a stream of Ar and cooled using a coldfinger condenser. After the irradiation, the solution was poured on water (150 mL) and extracted with Et$_2$O (3×20 mL). The combined extracts were washed with water (2×100 mL), dried over anhydrous MgSO$_4$, filtered, and the solvent was removed on a rotary evaporator. The crude product was purified on column of silica gel (10×1 cm) using CH$_2$Cl$_2$ as an eluent to regenerate starting compound (5 mg, 21%) and isolate product **9** (8 mg, 30%) in the form of yellowish film.

3-Azidomethyl-2-hydroxyanthacene (**9**): 8 mg (30 %); m.p. 201 °C (dec.); ^{1}H NMR (300 MHz, acetone-d_6) δ/ppm: 9.30 (br. s, 1H), 8.47 (s, 1H), 8.26 (s, 1H), 8.04 (s, 1H), 8.03-7.92 (m, 2H), 7.50-7.35 (m, 3H), 4.64 (s, 2H); ^{13}C NMR (150 MHz, acetone-d_6) δ/ppm: 155.0, 141.27, 141.25, 135.52, 135.46, 131.6, 130.7, 129.7, 128.6, 128.4, 127.6, 126.0, 125.2, 124.8, 110.1; IR (KBr) $\tilde{v}$/cm^{-1}: 3440, 2958, 2925, 2854, 1639, 1462, 1379, 892; HRMS-MALDI calcd. for C$_{15}$H$_{11}$N$_3$O (-e$^-$) 249.0900, found 249.0892.

Irradiation in the presence of N,C-protected cysteine 13

In a UV-vis cuvette (1×1 cm) was placed solution of compound **2** ($5×10^{-4}$ M, 3 mL) containing protected cysteine **13** ($5×10^{-2}$ M in CH$_3$CN-H$_2$O 9:1). The solution was purged with N$_2$ (30 min) and then irradiated in a Luzchem reactor with 8 lamps (350 nm, 8×8 W) for 20 min. HPLC analysis of the photoreaction mixture has proved that photoproduct is identical to the synthetically prepared sample.

Irradiation in the presence of lysine

In a UV-vis cuvvete (1×1 cm) was placed a solution of compound **2** ($1×10^{-4}$ M, 3 mL) containing of lysine (0.2 M in CH_3CN-H_2O 4:1). The solution was purged with N_2 (30 min) and then irradiated in a Luzchem reactor with 8 lamps (350 nm) for 40 min. The solvent was removed on a rotary evaporator and excess of lysine was removed by washing of the solid residue with water. After drying, the crude product was obtained in the form of orange-brown solid. Full characterization was not possible due to insolubility of the product.

3-(Acetoxymethyl)-2-acetoxyantracene (14)

Compound **2** (30 mg, 0.13 mmol) was dissolved in acetanhydride (5 mL) and pyridine was added (1 mL). The resulting solution was refluxed for 4 h, then was poured on CH_2Cl_2 (100 mL) in the extraction funnel. Organic phase was carefully shaken with sat. $NaHCO_3$ (150 mL) until bubbling ceased. Organic phase was separated, dried over $MgSO_4$, filtered and the solvent was removed on rotary evaporator. Crude product was purified on short plug of silica gel (5×0.5 cm) using CH_2Cl_2 as an eluent to give 38 mg (95%) of product **14** in the form of yellow solid.

3-(Acetoxymethyl)-2-acetoxyanthracene (14): 38 mg (95%); m.p. 189-191 °C; ^{1}H NMR (300 MHz, CDCl$_3$) δ/ppm: 8.44 (s, 1H), 8.37 (s, 1H), 8.07 (s, 1H), 7.98 (q, 2H, J = 8.0 Hz), 7.73 (s, 1H), 7.51-7.48 (m, 2H), 5.27 (s, 2H), 2.40 (s, 3H), 2.13 (s, 3H); ^{13}C NMR (150 MHz, CDCl$_3$) δ/ppm: 170.5 (s), 169.4 (s), 146.3 (s), 132.2 (s), 131.6 (s), 131.2 (s), 130.4 (d), 129.4 (s), 128.2 (d), 127.9 (d), 127.4 (s), 126.6 (d), 125.9 (d), 125.7 (d), 125.5 (d), 119.5 (d), 62.2 (t), 20.9 (q), 20.8 (q); IR (KBr) $\tilde{v}$/cm^{-1}: 3427 (vs), 3251 (vs), 2922 (s), 2853 (m), 1751 (vs), 1618 (s), 1560 (m), 1211 (m), 737 (m); HRMS-MALDI calcd. for $C_{19}H_{16}O_4$ (-e$^-$) 308.1050, found 308.1061.

(***R***)-Methyl-***N***-acetamidocysteinate (**13**) [62]. L-Cysteine hydrochloride-hydrate (5.07 g, 20 mmol) was suspended in the mixture of THF/H_2O (9:1, 10 mL) and NaOAc×$3H_2O$ (5.44 g, 40 mmol) was added with stirring. Through the next 1h, a solution of Ac_2O (2 mL) in THF/H_2O (9:1, 3 mL) was added. The resulting solution was stirred 16 h at rt under inert atmosphere (N_2), and after that 4 h at the reflux. To the cooled reaction mixture conc. HCl (2 mL) was added, followed by the addition of THF (50 mL), wherein NaCl precipitates. The resulting suspension was filtered and the filtrate was evaporated to dryness to give yellowish oil. Methanol (40 mL) was added, followed by the addition of sat. HCl in MeOH (5 mL). The resulting clear solution was refluxed for 1 h. After removal of the solvent on a rotary evaporator the crude product was obtained in the form of yellowish oil. Product was purified by chromatography on silica gel using CH_2Cl_2/EtOAc (1:1) as an eluent to give pure product **13** (2.13 g, 60 %) in the form of colorless oil, which solidifies upon standing in refrigerator. Characterisation is in accordance with previously reported [62].

(***R***)-Methyl-***N***-acetamidocysteinate (**13**): 2.13 g (60 %); ^{1}H NMR (300 MHz, $CDCl_3$) δ/ppm: 6.38 (br, s, 1H), 4.88-4.71 (m, 1H), 3.80 (s, 3H), 3.02 (ddd, 2H, J = 8.9, 4.0 and 1.0 Hz), 2.07 (s, 3H), 1.34 (t, 1H, J = 8.9 Hz).

(*R*)-Metyl-*N*-acetamido-*S*-((2-hydroxyanthracen-3-yl)methyl)cysteinate (10)

Diacetate **14** (31 mg, 0.1 mmol) was dissolved in dry CH_3CN (4 mL) and NaI (30 mg, 0.2 mmol) was added with stirring. In the inert atmosphere TMSCl (30 μL, 0.24 mmol) was added and the solution was heated on reflux. After 90 min of reflux, TLC analysis (SiO_2, CH_2Cl_2) showed that starting compound **14** was totally consumed and that one product was the main. Reaction mixture was poured on 0.3 M HCl (30 mL) in extraction funnel and then extracted with CH_2Cl_2

(3×15 mL). Combined extracts were dried on anhydrous Na_2SO_4, filtered and the solvent was removed on rotary evaporator. Crude product was purified by fast filtration trough short plug of silica gel (5×0.5 cm) using hexane/Et_2O (1:1) as an eluent to give 31 mg (82 %) of product **15** in the form of yellow solid. The compound rapidly decomposes on standing, especially if is exposed to light and air, so it was not completely characterized, but immediately used in the next step.

Protected cysteine **13** (20 mg, 0.11 mmol) was dissolved in CH_3CN (3 mL) under inert atmosphere (N_2) and DIPEA was added (30 µL, 0.17 mmol). Solution of **15** in CH_3CN (2 mL) was added dropwise. The resulting solution was stirred 15 min at rt and then at reflux for 2 h, whereupon was poured on 2% HOAc solution (30 mL) in the extraction funnel. Product was extracted with Et_2O (3×20 mL), combined extracts were dried over anhydrous Na_2SO_4, filtered and the solvent was removed on rotary evaporator. Product was purified by chromatography on silica gel using CH_2Cl_2 as an eluent and immediately used in the next step − removal of acetyl group from anthrol OH. Acetyl compound was dissolved in MeOH (5 mL) and 0.4 M solution of NaOMe in dry MeOH was added, which causes immediately color change to yellow. Stirring was continued of 15 min at rt under N_2 atmosphere. Reaction was quenched by pouring the reaction mixture on 10% HOAc (25 mL) in the extraction funnel. Product was extracted with Et_2O (3×20 mL). Combined extracts were dried over anhydrous Na_2SO_4, filtered and the solvent was removed on rotary evaporator. Product was purified by chromatography on silica gel using Et_2O as an eluent to give 8 mg (21% over 3 steps) of pure product **10** in the form of yellowish solid.

(*R*)-Methyl-*N*-acetamido-*S*-((2-hydroxyanthracen-3-yl)methyl)cysteinate (**10**): 8 mg (21% over 3 steps); m.p. 155-157 °C; ^{1}H NMR (300 MHz, $CDCl_3$) δ/ppm: 8.30 (s, 1H), 8.19 (s, 1H),

7.95-7.88 (m, 2H), 7.82 (s, 1H), 7.44-7.36 (m, 2H), 7.34 (s, 1H), 6.73 (br. s, 1H), 6.29 (br. d, 1H, J = 7.5 Hz), 4.93-4.88 (m, 1H), 4.07-3.96 (m, 2H), 3.73 (s, 3H), 3.05 (dd, 1H, J = 14 and 4.9 Hz), 2.90 (dd, 1H, J = 14 and 6 Hz), 2.00 (s, 3H); ^{13}C NMR (150 MHz, CDCl$_3$) δ/ppm: 171.2 (s), 170.3 (s), 152.0 (s), 132.3 (s), 132.1 (s), 130.4 (s), 130.0 (d), 129.1 (d), 127.9 (s), 127.5 (d), 126.6 (s), 125.9 (d), 125.5 (d), 124.5 (d), 123.5 (d), 109.8 (d), 52.7 (d), 51.6 (q), 33.7 (t), 32.8 (t), 23.0 (q); IR (KBr) $\tilde{v}$/cm^{-1}: 3423 (s), 3249 (s), 2922 (m), 2853 (w), 1751 (vs), 1618 (s), 1560 (m), 1211 (m), 737 (m); ESI-MS: (-) mode: m/z 382.1 [M−H$^+$], 239.0 [M−C$_6$H$_{10}$NO$_3$]$^-$; (+) mode: m/z 406.1 [M+Na$^+$], 384.1 [M+H$^+$]; HRMS-MALDI calcd. for C$_{21}$H$_{21}$NO$_4$S (-e$^-$) 383.1190, found 383.1173.

(S)-N_α-((2-hydroxy-3-anthracenyl)methyl)lysine (11) and (S)-N_γ-((2-hydroxy-3-anthracenyl)methyl)lysine (12)

Aldehyde **6** (50 mg, 0.23 mmol) and L-lysine (33 mg, 0.23 mmol) were suspended in a mixture of MeOH-CH$_2$Cl$_2$ (1:1, 30 mL) and the resulting suspension was stirred 4 h at rt. Then, NaBH$_3$CN (29 mg, 0.45 mmol) was added and the stirring was continued overnight at rt. The solvent was removed on a rotary evaporator to obtain the crude brown product. The remains of inorganic salts were washed with water (3×10 mL). Due to insolubility of products **11** and **12** in a variety of solvents and solvent mixtures, it was not possible to separate/purify them and take their NMR spectra. Therefore, they are characterized only by ESI-MS.

ESI-MS (+) mode: m/z calcd for [M+H$^+$] 353.2, found 353.3; calcd for [M-C$_6$H$_{13}$N$_2$O$_2$] 207.1, found 207.2.

3-Hydroxymethyl-1,2-anthraquinone (16)

Compound **2** (10 mg, 0.045 mmol) was dissolved in CH$_3$CN (50 mL) and water was added (50 mL). The resulting solution was purged with a stream of O$_2$ prior (20 min) and during the irradiation. A quartz tube was placed in Rayonet reactor and irradiated with 11 lamps at 350 nm. After 20 min of the irradiation, the solvent was removed on a rotary evaporator and the crude product was purified on a short column of silica gel using CH$_2$Cl$_2$/EtOAc (1:1) as an eluent to afford product **16** (8 mg, 75%) in the form of orange solid.

3-Hydroxymethyl-1,2-anthraquinone (**16**): 8 mg (75%); m.p. 185-188 °C; ^{1}H NMR (300 MHz, CDCl$_3$) δ/ppm: 8.64 (s), 7.97 (d, 1H, J = 8.0 Hz), 7.88 (d, 1H, J = 8.0 Hz), 7.77 (s, 1H), 7.70-7.57 (m, 3H), 4.60 (d, 2H, J = 4.9 Hz), ^{13}C NMR (150 MHz, CDCl$_3$) δ/ppm: 181.3 (s), 179.2 (s), 140.0 (d), 138.3 (s), 136.2 (s), 133.8 (d), 132.8 (s), 130.8 (d), 130.7 (d), 130.6 (d), 129.9 (s), 128.9 (d), 128.8 (d), 127.9 (s), 60.3 (q); IR (KBr) $\tilde{v}$/cm^{-1}: 3448 (s), 2922 (w), 2853 (w), 1691 (m), 1655 (vs), 1618 (vs), 1585 (m), 1450 (w), 1265 (w); HRMS-MALDI calcd. for C$_{15}$H$_{10}$O$_3$ (-e$^-$) 238.0630, found 238.0629.

1,2-Anthraquinone (**17**)

2-Anthrol (**3**) (15 mg, 0.077 mmol) was dissolved in CH$_3$CN (50 mL) and water was added (50 mL). The resulting solution was purged with a stream of O$_2$ prior (20 min) and during the irradiation. A quartz tube was placed in a Rayonet reactor and irradiated with 11 lamps at 350 nm. After 60 min irradiation, the solvent was removed on a rotary evaporator and the crude product was purified on a short column of silica gel using CH$_2$Cl$_2$ as an eluent to afford product **17** (10 mg, 62%) in the form of orange solid. Characterization is in accordance with previously published [30].

1,2-Anthraquinone (**17**) [30]: 10 mg (62 %); ^{1}H NMR (300 MHz, CDCl$_3$) δ/ppm: 8.68 (s, 1H), 7.99 (d, 1H, J = 7.9 Hz), 7.89 (d, 1H, J = 7.9 Hz), 7.95 (s, 1H), 7.72-7.58 (m, 3H), 6.53 (d, 1H, J = 10 Hz); ^{13}C NMR (150 MHz, DMSO-d$_6$) δ/ppm: 181.3 (s), 179.3 (s), 145.9 (d), 136.0 (s), 133.8 (d), 133.0 (s), 130.73 (d), 130.68 (d), 130.5 (d), 130.4 (s), 128.94 (d, 2C), 128.86 (s), 128.1 (d); ESI-MS: calcd for [M+H]$^+$ 209.1, found 209.2.

Anthraquinone-2-carboxylic acid (**18**)

2-Hydroxymethylanthracene (**4**) (20 mg, 0.096 mmol) was dissolved in CH$_3$CN (70 mL) and water was added (70 mL). The resulting solution was purged with stream of O$_2$ prior (20 min), and during the irradiation. Quartz tube was placed in Rayonet reactor and irradiated with s 11 lamps at 350 nm. After 45 min of irradiation, solvent was removed on rotary evaporator and crude product was purified on short column of silica gel using CH$_2$Cl$_2$/EtOAc (1:1) as an eluent to afford 17 mg (70 %) of product **18** in the form of orange solid. Characterization is in accordance with prevoiously published [63].

Anthraquinone-2-carboxylic acid (**18**) [63]: 17 mg (70 %); ^{1}H NMR (300 MHz, DMSO-d$_6$) δ/ppm: 13.7 (br. s, 1H), 8.65 (d, 1H, J = 1.7 Hz), 8.38 (dd, 1H, J = 8.1 and 1.7 Hz), 8.28 (d, 1H, J = 8.1 Hz), 8.24-8.19 (m, 2H), 7.96-7.92 (m, 2H); ^{13}C NMR (75 MHz, DMSO-d$_6$) δ/ppm: 182.1, 182.0, 166.0, 135.7, 134.8, 134.4, 133.3, 133.1, 127.4, 126.9.

Steady-State and Time-Resolved Fluorescence Measurements

Steady-state measurements were performed on a fluorimeter. The samples were dissolved in CH$_3$CN, or CH$_3$CN-H$_2$O (1:1) and the concentrations were adjusted to absorbances of less than 0.1 at the excitation wavelengths of 330, 350, and 370 nm. The solutions were purged with

nitrogen for 30 min prior to analysis. The measurements were performed at 20 °C. Fluorescence quantum yields were determined by comparison of the integral of the emission bands with the one of quinine sulfate in 0.05 M aqueous H_2SO_4 ($\Phi_F = 0.53$).[29] Typically, three absorption traces were recorded (and averaged) and three fluorescence emission traces were collected by exciting the sample at three different wavelengths. Three quantum yields were calculated (eq. S1 in the Supporting Information) and the mean value was reported.

UV-vis and fluorescence measurements with **2** in the presence of ct-DNA and BSA were conducted in CH_3CN-H_2O (1:9) in the presence of phosphate buffer (pH = 7, $c = 1\times10^{-3}$ M).

Fluorescence decays, collected over 1023 time channels, were obtained on a single photon counter using a pulsed laser at 375 nm. The instrument response functions, using LUDOX as the scatterer, were recorded at the same wavelengths as the excitation wavelength and had a half width of ≈ 90 ps. Emission decays for the samples were recorded until they reached 3×10^3 counts in the peak channel, at 410, 430 and 450 for in CH_3CN, and at 410, 450 and 550 nm in CH_3CN-H_2O. The time increment per channel was 0.024 ns. Obtained histograms were fit as sums of exponentials using global Gaussian-weighted non-linear least-squares fitting based on Marquardt-Levenberg minimization implemented in the Fast software package from the instrument. The fitting parameters (decay times and pre-exponential factors) were determined by minimizing the reduced chi-square χ^2 and graphical methods were used to judge the quality of the fit that included plots of the weighted residuals *vs.* channel number (for more details see the Supporting info.).

Laser Flash Photolysis (LFP)

All LFP studies were performed on a system previously described [64] using as an excitation source a pulsed Nd:YAG laser at 355 nm (<50 mJ per pulse), with a pulse width of 10 ns. Static cells (7 mm × 7 mm) were used and the solutions were purged with nitrogen or oxygen for 20 min prior to performing the measurements. Absorbances at 355 nm were ~0.3-0.5. For the collection of decays at long time scales, a modification of the setup was used, wherein the probing light beam from the Xe-lamp was not pulsed, as previously described [41].

Biological evaluation

Cell culture

The experiments were carried out on human carcinoma cell lines HCT-116 (colon), H460 (lung), MCF-7 and SUM 159 (breast), and HMLEshEcad/HMLEshGFP model. SUM 159, HMLEshEcad and HMLEshGFP cells were kindly provided by the Dr. Robert A. Weinberg laboratory (MIT). HCT-116, H460 and MCF-7 cells were cultured as monolayers and maintained in Dulbecco's modified Eagle medium (DMEM) supplemented with 10% fetal bovine serum (FBS) and 2mM L-glutamine. SUM159 cells (Asterand) were cultured in F12 + 5% FBS, insulin, and hydrocortisone. HMLE cells expressing either control shRNA (shGFP) or shRNA targeting E-cadherin (shEcad) were grown in a 1:1 mixture of DMEM + 10% FBS, insulin, hydrocortisone, and HuMEC ready medium. All cell lines were grown with the addition of 100 U/ml penicillin and 100 μg/ml streptomycin in a humidified atmosphere with 5% CO_2 at 37 °C.

Antiproliferative investigation

The cells were inoculated in parallel on two 96-well microtiter plates on day 0, at 3×10^4 cells/mL (H460, HCT-116), 4.5×10^4 cells/mL (MCF-7), 3.5×10^4 cells/mL (SUM 159), 2.5×10^4 cells/mL

(HMLEshEcad) or 2×10^4 cells/mL(HMLEshGFP). Test agents were added in ten-fold dilutions (10^{-8} to 10^{-4} M) on the next day and incubated for further 72 h. Working dilutions were freshly prepared on the day of testing. One of the plates was left in the dark, while the other was irradiated in a Luzchem reactor (6 lamps 350 nm, or 420 nm 5 min) at 4, 24, and 48 hours after the addition of the tested compounds. After 72 h of incubation the cell growth rate was evaluated by performing the MTT assay which detects dehydrogenase activity in viable cells. The absorbance (A) was measured on a microplate reader at 570 nm. The absorbance is directly proportional to the number of living, metabolically active cells. The percentage of growth (PG) of the cell lines was calculated according to expressions presented in the Supporting information. Each test was performed in quadruplicate in at least two individual experiments.

Cell cycle analysis

Cell lines HMLEshEcad and HMLEshGFP were seeded into 6-well plates (2×10^5 cells per well). After 24 hours, the tested compounds were added at various concentrations (as shown in the Results section). One of the plates was left in the dark, while the other was irradiated in a photoreactor (6 lamps, 420 nm, 5 min), 4 hours after the addition of the compounds. After 24 h, the attached cells were trypsinized, combined with floating cells, washed with phosphate buffer saline (PBS), fixed with 70% ethanol, and stored overnight at −20 °C. Immediately before analysis, the cells were washed with PBS and stained with 50 μg ml−1 of propidium iodide (PI) with the addition of 0.1 μg μl−1 of RNAse A. The stained cells were then analyzed by BD FACScalibur flow cytometer (20 000 counts were measured). The percentage of cells in each cell cycle phase was determined using FlowJo software (TreeStar Inc., USA). The tests were performed in duplicate and repeated at least twice.

Colony Forming Assay

Cells were plated at 200 cells per well (HMLEshEcad and HMLEshGFP), or 1000 cells per well (SUM159 and MCF-7) into 6-well plates. After 24 h, the tested compounds were added at various concentrations (as shown in the Results section). One of the plates was left in the dark, while the other was irradiated in a photoreactor (6 lamps, 420 nm, 5 min), 4 hours after the addition of the compounds. After 24 hours of treatment, cells were grown in fresh media as describe above, for additional 7 to 10 days depending on the cell line. After 7 to10 days cells were washed with ice cold PBS, fixed with methanol (-20 °C) and stained with 0.1 % crystal-violet for 10 minutes and rinsed with water. Colonies containing more than 50 cells were counted, and results were presented as Surviving fraction (SF), adapted from Franken *et al.*, 2006 [65]. Three independent experiments were performed.

Determination of ROS generation

Cell lines MCF-7, SUM159, HMLEshGFP and HMLEshEcad were plated in 24-well plates in duplicate (10000 cells per well). After 24 h, cells were treated with **3** and **4** both at 10^{-5} M and 10^{-6} M concentration. After two hours of incubation and 30 minutes before the irradiation 100 µl of 10 µM H2DCF-DA solution was added and of one of the plates was irradiated in photoreactor (Luzchem, 420nm, 5 min, 6 lamps). Immediately after the irradiation the solution was removed from both irradiated and non-irradiated plate and the cells were washed and trypsinized, then washed one more time in PBS and resuspended in 200 µl of PBS. The median fluorescent intensity of DCF in a minimum of 10000 cells was measured using a BD FACSCalibur™ flow

cytometer and analyzed in FlowJo software (TreeStar Inc., USA). Result was presented as a ratio of measured median fluorescence intensity (for more details see the Supporting information).

Confocal microscopy

Live cell confocal fluorescence microscopy was performed to assess the intracellular distribution of compounds with or without prior irradiation in photoreactor (420 nm, 5 min). Briefly, HMLEshEcad and HMELshGFP cells were seeded on round microscopic cover slips placed in 24-well-plates (10 000 cells/well) and grown at 37 °C for 24 h, as described above. Cells were then incubated with compounds **1**, **2**, **3** and **4** at various concentrations for 2 h. Cover slips were rinsed twice with PBS, placed on the microscopic slides and immediately analyzed. The uptake and intracellular distribution of tested chemicals were analyzed under Leica TCS SP2 AOBS confocal microscope (Leica Microsystems, Germany) with excitation wavelength 405 nm, emission detection: emission 1) 440-460 nm and emission 2) 540-560 nm.

Supporting information contains: selected experimental procedures and results, UV-vis and fluorescence spectra of **2**-**4**, LFP data and ^{1}H and ^{13}C NMR spectra. Supplementary data related to this article can be found online at http://..........

References:

[1] L.V. Nguyen, R.Vanner, P. Dirks, C.J. Eaves, Cancer stem cells: an evolving concept, Nat. Rev. Cancer 12 (2012) 133-143. https://doi.org/10.1038/nrc3184

[2] M.R. Alison, S.M.L. Lim, L.J. Nicholson, Cancer stem cells: problems for therapy? J. Pathol. 223 (2011) 147–161. https://doi.org/10.1002/path.2793

[3] P.B. Gupta, T.T. Onder, G.Jiang, K.Tao, C. Kuperwasser, R.A. Weinberg, E.S. Lander, Identification of selective inhibitors of cancer stem cells by high-throughput screening, Cell 138 (2009) 645–659. https://doi.org/10.1016/j.cell.2009.06.034

[4] O. Nagano, S. Okazaki, H. Saya, Redox regulation in stem-like cancer cells by CD44 variant Isoforms, Oncogene 32 (2013) 5191–5198. https://doi.org/10.1038/onc.2012.638

[5] E. Singer, J. Judkins, N. Salomonis, L. Matlaf, P. Soteropoulos, S. McAllister, L. Soroceanu, Reactive oxygen species-mediated therapeutic response and resistance in glioblastoma, Cell Death Dis. 6 (2015) e1601. https://doi.org/10.1038/cddis.2014.566

[6] D.E.J.G.J. Dolmans, D. Fukumura, R.K. Jain, Photodynamic therapy for cancer, Nature Rev. Cancer 3 (2003) 380-387. https://doi.org/10.1038/nrc1071

[7] J.T.-W. Wang, J.H. Woodharms, A.J. MacRobert, S.G. Bown, K. Berg, Photodynamic therapy, In CRC Handbook of Organic Photochemistry and Photobiology, A.G. Griesbeck, M. Oelgemöller, F. Ghetti (Eds.), CRC Press, Boca Raton, 2012, pp 1529-1540.

[8] C. Conway, S.B. Brown, Photodynamic drug delivery, In CRC Handbook of Organic Photochemistry and Photobiology, A.G. Griesbeck, M. Oelgemöller, F. Ghetti (Eds.), CRC Press, Boca Raton, 2012, pp 1511-1528.

[9] L. Cheng, C. Wang, L. Feng, K. Yang, Z. Liu, Functional Nanomaterials for Phototherapies of Cancer, Chem. Rev. 114 (2014) 10869-10939. https://doi.org/10.1021/cr400532z

[10] S. Vinogradov, X. Wei, Cancer stem cells and drug resistance: the potential of nanomedicine, Nanomedicine 7 (2012) 597–615. https://doi.org/10.2217/nnm.12.22

[11] S.E. Rokita (Ed.), Quinone Methides, Wiley, Hoboken, 2009.

[12] M. Freccero, Quinone Methides as Alkylating and Cross-Linking Agents, Mini Rev. Org. Chem. 1 (2004) 403-415. https://doi.org/10.2174/1570193043403091

[13] P. Wang, Y. Song, L. Zhang, H. He, X. Zhou, Quinone Methide Derivatives: Important Intermediates to DNA Alkylating and DNA Cross-linking Actions, Curr. Med. Chem. 12 (2005) 2893-2913. https://doi.org/10.2174/092986705774454724

[14] N. Basarić, K. Mlinarić-Majerski, M. Kralj, Quinone Methides: Photochemical Generation and its Application in Biomedicine, Curr. Org. Chem. 18 (2014) 3-18. https://doi.org/10.2174/138527281801140121122330

[15] C. Percivalle, F. Doria, M. Freccero, Quinone Methides as DNA Alkylating Agents: An Overview on Efficient Activation Protocols for Enhanced Target Selectivity, Curr. Org. Chem. 18 (2014) 19-43. https://doi.org/10.2174/13852728113176660135

[16] H. Wang, Quinone Methides and Their Biopolymer Conjugates as Reversible DNA Alkylating Agents, Curr. Org. Chem. 18 (2014) 44-60. https://doi.org/10.2174/138527281801140121122736

[17] E. Modica, R. Zanaletti, M. Freccero, M. Mella, Alkylation of Amino Acids and Glutathione in Water by *o*-Quinone Methide. Reactivity and Selectivity, J. Org. Chem. 66 (2001) 41-52. https://doi.org/10.1021/jo0006627

[18] S. Arumugam, J. Guo, N.E. Mbua, F. Friscourt, N. Lin, E. Nekongo, G.-J. Boons, V.V. Popik, Selective and reversible photochemical derivatization of cysteine residues in peptides and proteins, Chem. Sci. 5 (2014) 1591-1598. https://doi.org/10.1039/c3sc51691a

[19] M. Kralj, L. Uzelac, Y.-H. Wang, P. Wan, M. Tireli, K. Mlinarić-Majerski, I. Piantanida, N. Basarić, Enhancement of antiproliferative activity by phototautomerization of anthrylphenols, Photochem. Photobiol. Sci. 14 (2015) 1082-1092. https://doi.org/10.1039/c5pp00099h

[20] Đ. Škalamera, C. Bohne, S. Landgraf, N. Basarić, Photodeamination Reaction Mechanism in Aminomethyl *p*-Cresol Derivatives: Different Reactivity of Amines and Ammonium Salts, J. Org. Chem. 80 (2015) 10817-10828. https://doi.org/10.1021/acs.joc.5b01991

[21] D. Verga, M. Nadai, F. Doria, C. Percivalle, M. Di Antonio, M. Palumbo, S.N. Richter, M. Freccero, Photogeneration and Reactivity of Naphthoquinone Methides as Purine Selective DNA Alkylating Agents, J. Am. Chem. Soc. 132 (2010) 14625-14637. https://doi.org/10.1021/ja1063857

[22] F. Doria, S.N. Richter, M. Nadai, S. Colloredo-Mels, M. Mella, M. Palumbo, M. Freccero, BINOL−Amino Acid Conjugates as Triggerable Carriers of DNA-Targeted Potent Photocytotoxic Agents, J. Med. Chem. 50 (2007) 6570-6579. https://doi.org/10.1021/jm070828x

[23] L. Diao, C. Yang, P. Wan, Quinone Methide Intermediates from the Photolysis of Hydroxybenzyl Alcohols in Aqueous Solution, J. Am. Chem. Soc. 117 (1995) 5369-5370. https://doi.org/10.1021/ja00124a024

[24] J. Veljković, L. Uzelac, K. Molčanov, K. Mlinarić-Majerski, P. Wan, N. Basarić, Sterically Congested Adamantylnaphthalene Quinone Methides, J. Org. Chem. 77 (2012) 4596-4610. https://doi.org/10.1021/jo3002479

[25] Đ. Škalamera, K. Mlinarić-Majerski, I. Martin-Kleiner, M. Kralj, P. Wan, N. Basarić, Near-Visible Light Generation of a Quinone Methide from 3-Hydroxymethyl-2-anthrol, J. Org. Chem. 79 (2014) 4390-4397. https://doi.org/10.1021/jo500290y

[26] Đ. Škalamera, K. Mlinarić-Majerski, I. Martin-Kleiner, M. Kralj, J. Oake, P. Wan, C. Bohne, N. Basarić, Photochemical formation of anthracene quinone methide derivatives, J. Org. Chem. 2017 in press. https://doi.org/10.1021/acs.joc.6b02735

[27] F. Doria, A. Lena, R. Bargiggia, M. Freccero, Conjugation, Substituent, and Solvent Effects on the Photogeneration of Quinone Methides, J. Org. Chem. 81 (2016) 3665-3673. https://doi.org/ 10.1021/acs.joc.6b00331

[28] M. Nadai, F. Doria, L. Germani, S. N. Richter, M. Freccero, A Photoreactive G-Quadruplex Ligand Triggered by Green Light, Chem Eur. J. 21 (2015) 2330-2334. https://doi.org/ 10.1002/chem.201405215

[29] M. Montalti, A. Credi, L. Prodi, M.T. Gandolfi, In Handbook of Photochemistry, CRC Taylor and Francis: Boca Raton, 2006.

[30] K. Krohn, H. Rieger, K. Khanbabaee, A new synthesis of *ortho*-Quinones by transition-metal-mediated oxygenation of phenols with tert-butylhydroperoxide and the mimoun oxodiperoxo molybdenum complex [Mo(O$_2$)$_2$O] · Py · HMPT, Chem. Ber. 122 (1989) 2323-2330. https://doi.org/10.1002/cber.19891221220

[31] S. Goldstein, J. Rabani, The ferrioxalate and iodide–iodate actinometers in the UV region, J. Photochem. Photobiol. A: Chem 193 (2008) 50-55. https://doi.org/10.1016/j.jphotochem.2007.06.006

[32] H.J. Kuhn, S.E. Braslavsky, R. Schmidt, Chemical Actinometry, Pure Appl. Chem. 76 (2004) 2105-2146. https://doi.org/10.1351/pac200476122105

[33] J. Lee, G.W. Robinson, S.P. Webb, L.A. Philips, J.H. Clark, Hydration dynamics of protons from photon initiated acids, J. Am. Chem. Soc. 108 (1986) 6538-6542. https://doi.org/10.1021/ja00281a016

[34] L.M. Tolbert, J.E. Haubrich, Photoexcited Proton Transfer from Enhanced Photoacids, J. Am. Chem. Soc. 116 (1994) 10593-10600. https://doi.org/10.1021/ja00102a028

[35] R.W. Van de Water, T.R.R., Pettus, *o*-Quinone methides: intermediates underdeveloped and underutilized in organic synthesis, Tetrahedron 58 (2002) 5367-5405. https://doi.org/10.1016/S0040-4020(02)00496-9

[36] G.A. Olah, S.C. Narang, B.G. Balaram Gupta, R. Malhotra, Synthetic methods and reactions. 62. Transformations with chlorotrimethylsilane/sodium iodide, a convenient in situ iodotrimethylsilane reagent, J. Org. Chem. 44 (1979) 1247-1251. https://doi.org/10.1021/jo01322a012

[37] W.T. Dixon, D. Murphy, Determination of the acidity constants of some phenol radical cations by means of electron spin resonance, J. Chem. Soc. Faraday Trans. 2 72 (1976) 1221-1230. https://doi.org/10.1039/F29767201221

[38] F.G. Brodwell, J.-P. Cheng, Substituent effects on the stabilities of phenoxyl radicals and the acidities of phenoxyl radical cations, J. Am. Chem. Soc. 113 (1991) 1736-1743. https://doi.org/10.1021/ja00005a042

[39] T.A. Gadosy, D. Shukla, L.J., Johnston, Generation, Characterization, and Deprotonation of Phenol Radical Cations, J. Phys. Chem. A 103 (1999) 8834-8839. https://doi.org/10.1021/jp992216x

[40] M. Fischer, P. Wan, Nonlinear Solvent Water Effects in the Excited-State (Formal) Intramolecular Proton Transfer (ESIPT) in *m*-Hydroxy-1,1-diaryl Alkenes: Efficient Formation of *m*-Quinone Methides, J. Am. Chem. Soc. 121 (1999) 4555-4562. https://doi.org/10.1021/ja983557b

[41] R.H. Mitchell, C. Bohne, Y. Wang, S. Bandyopadhyay, C.B. Wozniak, Multistate π Switches: Synthesis and Photochemistry of a Molecule Containing Three Switchable Annelated Dihydropyrene Units, J. Org. Chem. 71 (2006) 327-336. https://doi.org/10.1021/jo052153g

[42] M.H. Kleinman, J.H. Flory, D.A. Tomalia, N.J., Turro, Effect of Protonation and PAMAM Dendrimer Size on the Complexation and Dynamic Mobility of 2-Naphthol, J. Phys. Chem. B 104 (2000) 11472-11479. https://doi.org/10.1021/jp001882r

[43] L. Pretali, F. Doria, D. Verga, A. Profumo, M. Freccero, Photoarylation/Alkylation of Bromonaphthols, J. Org. Chem. 74 (2009) 1034-1041. https://doi.org/10.1021/jo802374r

[44] D. Brousmiche, M. Xu, M. Lukeman, P. Wan, Photohydration and Photosolvolysis of Biphenyl Alkenes and Alcohols via Biphenyl Quinone Methide-type Intermediates and Diarylmethyl Carbocations, J. Am. Chem. Soc. 125 (2003) 12961-12970. https://doi.org/10.1021/ja036808b

[45] R.A. McClelland, C. Chan, F.L. Cozens, A. Modro, S. Steenken, Laser Flash Photolysis Generation, Spectra, and Lifetimes of Phenylcarbenium Ions in Trifluoroethanol and Hexafluoroisopropyl Alcohol. On the UV Spectrum of the Benzyl Cation, Angew. Chem. Int. Ed. 30 (1991) 1337-1339. https://doi.org/10.1002/anie.199113371

[46] F.L. Cozens, V.M. Kanagasabapathy, R.A. McClelland, S. Steenken, Lifetimes and UV-visible absorption spectra of benzyl, phenethyl, and cumyl carbocations and corresponding vinyl cations. A laser flash photolysis study, Can. J. Chem. 77 (1999) 2069-2082. https://doi.org/10.1139/v99-210

[47] C.M. Fillmore, C. Kuperwasser, Human breast cancer cell lines contain stem-like cells that self-renew, give rise to phenotypically diverse progeny and survive chemotherapy, Breast Cancer Res. 10 (2008) R25. https://doi.org/ 10.1186/bcr1982

[48] D. Mikulski, R. Górniak, M. Molski, A theoretical study of the structure–radical scavenging activity of trans-resveratrol analogues and cis-resveratrol in gas phase and water environment, Eur. J. Med. Chem. 45 (2010) 1015-1027. https://doi.org/10.1016/j.ejmech.2009.11.044

[49] G.T. Charras, A Short History of Blebbing. J. Microsc. 231 (2008) 466–78. https://doi.org/ 10.1111/j.1365-2818.2008.02059.x

[50] L.F. Barros, T. Kanaseki, R. Sabirov, S. Morishima, J. Castro, C.X. Bittner, E. Maeno, Y. Ando-Akatsuka, Y. Okada, Apoptotic and necrotic blebs in epithelial cells display similar neck diameters but different kinase dependency, Cell Death Differ. 10 (2003) 687–697. https://doi.org/10.1038/sj.cdd.4401236

[51] A.M. Crous, H. Abrahamse, Lung cancer stem cells and low-intensity laser irradiation: a potential future therapy?, Stem Cell Res. Ther. 4 (2013) 129. https://doi.org/10.1186/scrt340

[52] A.P. Castano, T.N. Demidova, M.R. Hamblin, Mechanisms in photodynamic therapy: part one-photosensitizers, photochemistry and cellular localization. Photodiagnosis Photodyn. Ther. 1 (2004) 279–293. https://doi.org/ 10.1016/S1572-1000(05)00007-4

[53] A.P. Castano, T.N. Demidova, M.R. Hamblin, Mechanisms in photodynamic therapy: part two-cellular signaling, cell metabolism and modes of cell death. Photodiagnosis Photodyn. Ther. 2 (2005) 1-23. http://doi.org/10.1016/S1572-1000(05)00030-X

[54] L. Li, H. Wang, H. Wang, L. Li, P. Wang, X. Wang, Q. Liu, Interaction and oxidative damage of DVDMS to BSA: a study on the mechanism of photodynamic therapy-induced cell death. Sci. Rep. 7 (2017) 43324. https://doi.org/10.1038/srep43324

[55] S. Arumugam, V.V. Popik, Photochemical Generation and the Reactivity of *o*-Naphthoquinone Methides in Aqueous Solutions, J. Am. Chem. Soc. 131 (2009) 11892-11899. https://doi.org/10.1021/ja9031924

[56] X. Sun, W.N. Leung, Photodynamic Therapy with Pyropheophorbide-a Methyl Ester in Human Lung Carcinoma Cancer Cell: Efficacy, Localization and Apoptosis, Photochem. Photobiol 75 (2002) 644–651. https://doi.org/10.1562/0031-8655(2002)0750644PTWPAM2.0.CO2

[57] Y. Feng, E.S. Sokol, P.B. Gupta, The endoplasmic reticulum may be an Achilles' heel of cancer cells that have undergone an epithelial-to-mesenchymal transition. Mol Cell Oncol. 1 (2014) e961822. https://doi.org/10.4161/23723548.2014.961822

[58] G.T. Wondrak, Redox-Directed Cancer Therapeutics: Molecular Mechanisms and Opportunities, Antioxid Redox Signal. 11 (2009) 3013-69. https://doi.org/10.1089/ars.2009.2541

[59] G.-Y. Liou, P. Storz,. Reactive oxygen species in cancer, Free Radic Res. 44 (2010) 479-496. https://doi.org/10.3109/10715761003667554

[60] Maiti, A. K. Reactive Oxygen Species Reduction is a Key Underlying Mechanism of Drug Resistance in Cancer Chemotherapy. Chemotherapy 1:104 (2012) https://doi.org/10.4172/2167-7700.1000104

[61] P. Mroz, A. Yaroslavsky, G.B. Kharkwal, M.R. Hamblin, Cell death pathways in photodynamic therapy of cancer, Cancers 3 (2011) 2516-2539. https://doi.org/10.3390/cancers3022516.

[62] C.E. Aroyan, A. Dermenci, S.J., Miller, Development of a Cysteine-Catalyzed Enantioselective Rauhut−Currier Reaction, J. Org. Chem. 75 (2010) 5784-5796. https://doi.org/10.1021/jo101018t

[63] sdbs.db.aist.go.jp/sdbs/ (accessed Oct 2014)

[64] Y. Liao, C. Bohne, Alcohol Effect on Equilibrium Constants and Dissociation Dynamics of Xanthone−Cyclodextrin Complexes, J. Phys. Chem. 100 (1996) 734-743. https://doi.org/10.1021/jp951697r

[65] N.A. Franken, H.M. Rodermond, J. Stap, J. Haveman, C. van Bree, Clonogenic Assay of Cells in Vitro, Nature Protocols 1 (2006) 2315-2319. https://doi.org/10.1038/nprot.2006.339